Magnetic domain walls in single-phase and phase-separated double-exchange systems

D. I. Golosov*

Theoretical Physics, Oxford University, 1 Keble Road, Oxford OX1 3NP, United Kingdom

We investigate the structure of magnetic domain walls in a classical double-exchange ferromagnet, evaluating domain wall energies and charges. Three different cases are studied: (i) a conventional smooth Bloch wall, (ii) an abrupt Ising-type wall, which is shown to have lower energy at small values of carrier concentration, and (iii) stripe wall, corresponding to the two ferromagnetic domains being separated by a stripe of another, antiferromagnetic, phase. General aspects of energy balance and geometry of phase-separated states are discussed in this context. It is speculated that domain walls of the latter type may be responsible for the unusual transport properties of certain manganate films.

I. INTRODUCTION

The unusual micromagnetic properties of colossal magnetoresistance (CMR) compounds are presently subject to intensive experimental investigation.[1–11] In these studies, special attention is paid to the interplay between magnetic domain structure and transport properties of the system. Aside from possible technological applications (associated with the large low-field magnetoresistance[6]), the strong effect of magnetic domain walls on conduction properties, as found in strained epitaxial films of $La_{0.7}Ca_{0.3}MnO_3$ (Refs. 5 and 6), $Pr_{2/3}Sr_{1/3}MnO_3$ (Ref. 6), and $La_{0.7}Sr_{0.3}MnO_3$ (Refs. 6 and 7), raises a genuine physical problem. Indeed, given the relatively small expected value of the easy-axis magnetic anisotropy, the usual Bloch (or Néel) domain wall would be rather smooth and broad. Thus, carrier scattering off the Bloch walls could not appreciably affect transport properties of the system. The measurement of the magnetic domain wall contribution to the resistivity therefore leads to the conclusion[12] that the domain walls arising in the samples studied in Refs. 5–7 have an unusual, non-Bloch structure. It has even been suggested[6] that the double-exchange interaction, which is responsible for the ferromagnetism of doped manganese oxides, cannot possibly account for such poorly conducting magnetic domain walls. While the origins of this suggestion may be traced to the widespread but ill-founded notion that the magnetic properties of double-exchange systems can be adequately described by an effective Heisenberg model, the peculiar physics of domain walls in double-exchange ferromagnets has not yet been addressed theoretically.

In the present article, we consider the standard single-orbital double-exchange model with the following Hamiltonian:

$$\mathcal{H} = -\frac{t}{2} \sum_{\langle i,j \rangle, \alpha} (c_{i\alpha}^\dagger c_{j\alpha} + c_{j\alpha}^\dagger c_{i\alpha}) - \frac{J_H}{2S} \sum_{i,\alpha,\beta} \vec{S}_i \cdot \vec{\sigma}^{\alpha\beta} c_{i\alpha}^\dagger c_{i\beta}$$

$$+ \frac{J}{S^2} \sum_{\langle i,j \rangle} \vec{S}_i \cdot \vec{S}_j - \frac{K}{2S^2} \sum_i (S_i^z)^2. \qquad (1)$$

Here $c_{j\alpha}$ (with $\alpha = \uparrow, \downarrow$) are the electron annihilation operators, and the vector $\vec{\sigma}^{\alpha\beta}$ is composed of Pauli matrices. J_H is the strength of Hund's rule ferromagnetic coupling between the spins of carriers and the core spins $\vec{S}_i$, which also interact with each other via the direct antiferromagnetic Heisenberg exchange J. The core spins are assumed to be classical ($S \gg 1$), and the easy-axis single-ion anisotropy K/S^2 is included in order to account for the finite Bloch wall energy. The lattice is assumed to be square, which is thought to be more appropriate than the three-dimensional cubic one for modeling the thin films studied experimentally; the extension of our analysis to the three-dimensional case is straightforward but cumbersome, and is expected to yield similar conclusions. The electron spectrum in the ferromagnetic state is given by[13] $\epsilon_{\vec{k}}^{\uparrow,\downarrow} = \epsilon_{\vec{k}} \mp J_H/2$ with $\epsilon_{\vec{k}} = -t(\cos k_1 + \cos k_2)$. We consider the experimentally relevant *half-metallic* case, when owing to a sufficiently large value of J_H, the carrier band in the ferromagnetic phase is completely spin polarized. Thus the value of chemical potential, denoted $\mu - J_H/2$, must lie below the bottom of the spin-up subband, $\mu < J_H - 2$. We note that t in Eq. (1) corresponds to $2t$ in a different notation sometimes used elsewhere in the literature; it should also be pointed out that below, the conduction electron (rather than hole) density is denoted by x. Throughout the paper we use units in which hopping t and the lattice spacing are equal to unity, and we consider the zero-temperature ($T=0$) case.

Below we consider domain walls of three different types, which are relevant for different values of parameters characterizing the double-exchange magnet at low temperatures. These are conventional Bloch walls, abrupt (Ising) walls, and stripe walls, formed by a stripe of antiferromagnetic phase inserted between the two ferromagnetic domains.

We begin in Sec. II with the usual smooth Bloch wall. The Bloch wall energy depends on spin stiffness D and anisotropy strength in a usual way,[14] reflecting the fact that the long-wavelength properties of double-exchange ferromagnets are adequately captured within an effective Heisenberg description (cf. Ref. 15). In double-exchange systems, Bloch walls carry an electric charge, which we also evaluate. Our results suggest that magnetic domain walls arising in homogeneous (single-phase) double-exchange ferromagnets at the intermediate doping levels typically have Bloch structure, and therefore cannot significantly affect the resistance of the sample.

Within the context of recent experiments, the possibility of sharp changes in magnetization direction within a domain wall is of particular relevance. This scenario has been discussed for a long time (see, e.g., Ref. 16) and it is important to consider it in some detail. Therefore in Sec. III we treat the extreme case of an abrupt (Ising-type) domain wall, when the sign of magnetization is reversed over one lattice link. A wall of this type, which in the $T=0$, $S\rightarrow\infty$ limit is impenetrable for carriers, would strongly affect the transport properties of the system. The energy cost of an abrupt wall originates from the underlying nonperturbative scattering problem for conduction electrons. The corresponding physics is thus completely non-Heisenberg. We derive expressions for energies and charges of abrupt domain walls running in two different directions (along a crystal axis and diagonally) and for all values of the Hund's rule exchange constant J_H. While for small values of carrier density, $x\ll1$, the energy of an abrupt wall is lower than that of a Bloch wall (which may be relevant for certain magnetic semiconductors), this does not generally hold at the intermediate doping levels. In the latter case, an abrupt domain wall is preferred only for very large values of anisotropy, $K\sim DS$, or for the case of very finely tuned parameter values, providing for an almost exact balance between the ferro- and antiferromagnetic tendencies of the system. It would be unrealistic to expect that such a fine-tuning (within 1% in the values of J, J_H, and x in a single-phase system) can be achieved by different experimental groups in a reproducible way.

In addition, it also turns out that these parameter values typically correspond to the system being unstable with respect to phase separation. As explained in Sec. IV, the latter phenomenon has a double effect: (i) the carrier density within the bulk of the ferromagnet is now determined by the condition that the thermodynamic potentials of the two phases must be equal to each other; this condition effectively pins the parameters of the double-exchange ferromagnet in the region where the energy of an abrupt domain wall is relatively low. (ii) The energy of an abrupt domain wall can be further lowered by inserting a stripe of antiferromagnetic phase between the two ferromagnetic domains. Since the two phases are characterized by different values of charge density, one cannot treat this situation properly without taking into account the effects of Coulomb interaction. We use a somewhat simplified treatment to estimate the energy and width of a stripe domain wall. It turns out that within a certain range of parameter values, the energy of a stripe wall can be lower than that of a Bloch wall, so that magnetic domain walls in a phase-separated system are actually of the stripe type. In particular, this situation is realized when the antiferromagnetic phase occupies an appreciable area of the sample (of the order of 15% of the net area, or possibly more), provided that the easy-axis anisotropy constant K is not too small. Due to insulating properties of the antiferromagnetic phase, carrier transport across the stripe wall is strongly suppressed, leading to a substantial domain wall contribution to the sample resistance. On the other hand, the ferromagnetic area within a single magnetic domain remains well connected, and phase separation is therefore not expected to significantly affect the *intradomain* metallic conductivity. Analysis of the data of Refs. 5 and 6 reveals a correlation between the film thickness, dielectric properties of the substrate, and the appearance of domain wall resistance, which seems to agree with the anticipated conditions for the stabilization of the stripe walls.

Details of calculations are relegated to the Appendixes, which also include a brief discussion of the three-dimensional (3D) case.

The relevance of our findings in the context of recent experiments on manganate films is further discussed in Sec. V. We suggest that the domain walls observed indirectly in the transport measurements of Refs. 5–7 and directly in Ref. 8 are in fact the stripe walls, introduced in Sec. IV.

II. BLOCH WALL

The structure of domain walls in conventional Heisenberg ferromagnets was understood long ago.[14] These are smooth, long-wavelength Bloch walls,[17] and their surface tension (energy per unit length) S_B and width l_B are determined by the spin stiffness D of the system:

$$S_B=2\sqrt{K(DS)}, \quad l_B=\sqrt{DS/K}. \tag{2}$$

Since the unusual transport properties of the domain walls are found only in certain strained films at a specific doping level,[5–7] we expect that in most cases, domain walls in the CMR materials also have Bloch-like structure. We will now study the relationship between the properties of Bloch walls and the parameters of our model Hamiltonian, Eq. (1).

The appropriate value of D can be extracted from the known spin-wave spectrum of a classical double-exchange ferromagnet[18] (see also Ref. 15):

$$\omega_{\vec{p}}=\frac{J_H}{2NS}\sum_{\vec{k}} n_{\vec{k}}\frac{\epsilon_{\vec{k}}-\epsilon_{\vec{k}+\vec{p}}}{\epsilon_{\vec{k}}^{\uparrow}-\epsilon_{\vec{k}+\vec{p}}^{\downarrow}}+\frac{K}{S}+\frac{2J}{S}\sum_{\alpha=1}^{d}(\cos k_\alpha-1). \tag{3}$$

Here, N is the number of lattice sites, and $n_{\vec{p}}$ is the Fermi distribution function. Equation (3) is valid for any dimensionality d and for an arbitrary electron dispersion law $\epsilon_{\vec{k}}$ (with $\epsilon_{\vec{k}}^{\uparrow,\downarrow}=\mp J_H/2+\epsilon_{\vec{k}}$). For the case of the 2D tight-binding model (1), we obtain

$$SD=-J+\left(\frac{|E|}{8}-\frac{1}{4J_H N}\sum_{\vec{k}} n_{\vec{k}}v_{\vec{k}}^2\right)$$

$$=-J-\frac{x}{4J_H}-\frac{\mu}{8\pi^2}\left(\mu-\frac{2+\mu^2}{J_H}\right)Y_1$$

$$+\frac{1}{4\pi^2}\left(2-\frac{3\mu}{J_H}\right)Y_2. \tag{4}$$

Here and below, Y_1 and Y_2 denote the following complete elliptic integrals:

$$Y_1=\mathcal{K}\left(\sqrt{1-\frac{1}{4}[\mu(x)]^2}\right), \quad Y_2=\mathcal{E}\left(\sqrt{1-\frac{1}{4}[\mu(x)]^2}\right), \tag{5}$$

$\vec{v}_{\vec{k}} = \partial \epsilon_{\vec{k}} / \partial \vec{k}$ is the electron velocity, and the kinetic energy of the band is given by

$$E \equiv \frac{1}{N} \sum_{\vec{k}} n_{\vec{k}} \epsilon_{\vec{k}} = \frac{\mu^2}{\pi^2} Y_1(x) - \frac{4}{\pi^2} Y_2(x). \qquad (6)$$

Note that because of the numerical prefactor entering Eq. (4), the value of D is at least an order of magnitude smaller than that of the band energy, E.

At low doping level $x \ll 1 \lesssim J_H$, Eq. (4) yields

$$DS = -J + \frac{1}{4}x - \frac{1}{8}\pi x^2 - \frac{\pi x^2}{2J_H}, \qquad (7)$$

whereas at half-filling $x = 1$, we obtain

$$DS = -J - 1/(4J_H). \qquad (8)$$

The second term in Eq. (7), which is proportional to the band energy ($E \approx -2x$ at low x), represents the leading-order double-exchange (ferromagnetic) contribution. The last terms in Eqs. (7) and (8) indicate that the effect of finite J_H (as opposed to $J_H \to \infty$) is similar to that of an increase in the value of direct superexchange, J. This conclusion is justified physically, since at finite J_H an effective antiferromagnetic interaction arises due to virtual transitions between the two components of the spin-split band much like a usual superexchange, which is due to transitions between different bands. Below we will see how this qualitative analogy[19] manifests itself in other properties of the system—its validity is clearly not restricted to the spin stiffness evaluation. This in turn suggests that many of the features of (more complicated) finite-J_H systems can be modeled by treating the $J_H \to \infty$ case with an appropriately increased J.

The doping dependence of the spin stiffness for three different values of J_H ($J_H \to \infty$, $J_H = 8$, and $J_H = 4$ for solid, dashed, and dash-dotted lines, respectively) and $J = 0$ is shown in Fig. 1(a). For the case of finite J_H, the competition between effective antiferromagnetism and double-exchange-induced ferromagnetism, taking place at sufficiently small $1 - x$, is resolved via phase separation.[20–23] This means that the homogeneous ferromagnetic state becomes thermodynamically unstable as the electron concentration x exceeds a certain critical value. In Fig. 1(a), the values of DS within the respective thermodynamically unstable regions are plotted with dotted lines. When the superexchange $J > 0$ is present, this critical value, which depends also on J_H, decreases further. In addition, another region of phase-separation instabilities arises at low *electron* densities.[21,22]

Within a Bloch wall, misalignment of the neighboring ionic spins leads to a renormalisation of carrier hopping coefficient.[24] Indeed, the Hamiltonian (1) can be rewritten in terms of new fermions $d_{i\uparrow}$ (and $d_{i\downarrow}$), whose spin is aligned (antialigned) with the classical ionic spin $\vec{S}_i$ at the same site:
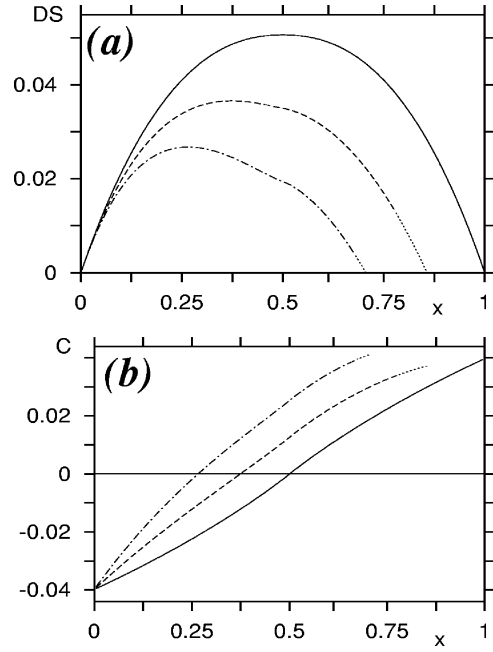

FIG. 1. Spin stiffness DS (a) and the coefficient $\mathcal{C}$ [see Eq. (19)] (b) vs electron density x for $J = 0$ and $J_H \to \infty$ (solid line), $J_H = 8$ (dashed line), and $J_H = 4$ (dash-dotted line). Dotted lines correspond to a regime where the spin stiffness is still positive, $D > 0$, but the ferromagnetic phase is unstable with respect to phase separation.

$$\mathcal{H} = -\frac{1}{2} \sum_{\langle i,j \rangle, \alpha, \beta} (t_{ij}^{\alpha\beta} d_{i\alpha}^\dagger d_{j\beta} + t_{ji}^{\alpha\beta} d_{j\alpha}^\dagger d_{i\beta})$$

$$+ \frac{J_H}{2} \sum_i (d_{i\downarrow}^\dagger d_{i\downarrow} - d_{i\uparrow}^\dagger d_{i\uparrow}) + \frac{J}{S^2} \sum_{\langle i,j \rangle} \vec{S}_i \cdot \vec{S}_j$$

$$- \frac{K}{2S^2} \sum_i (S_i^z)^2. \qquad (9)$$

Here, the matrix $t^{\alpha\beta}$ is given by

$$t_{ij}^{\alpha\beta} = \begin{pmatrix} \widetilde{C}_i \widetilde{C}_j + e^{i(\phi_j - \phi_i)} \widetilde{S}_i \widetilde{S}_j & -e^{-i\phi_j} \widetilde{C}_i \widetilde{S}_j + e^{-i\phi_i} \widetilde{S}_i \widetilde{C}_j \\ -e^{i\phi_i} \widetilde{S}_i \widetilde{C}_j + e^{i\phi_j} \widetilde{C}_i \widetilde{S}_j & \widetilde{C}_i \widetilde{C}_j + e^{i(\phi_i - \phi_j)} \widetilde{S}_i \widetilde{S}_j \end{pmatrix},$$

$$\widetilde{C}_i = \cos\frac{\theta_i}{2}, \quad \widetilde{S}_i = \sin\frac{\theta_i}{2}, \qquad (10)$$

and θ_i, ϕ_i are the polar coordinates of the spin $\vec{S}_i$.

In the bulk of the ferromagnetic state, $t_{ij}^{\alpha\beta}$ reduces to a unit matrix, but inside the domain walls, the values of both diagonal and off-diagonal elements are changed. Thus, the band structure (and hence the carrier density) within the wall differs from that in the bulk, and we come to the conclusion that *Bloch walls are charged*. We will now evaluate the surface charge σ_B of a Bloch wall in a double-exchange ferromagnet.

Let us suppose that the Bloch wall runs along the [11] direction of the lattice diagonal, and choose the y axis to be perpendicular to the wall. We also choose the coordinates in

spin space in such a way that $\phi_i \equiv 0$, and note that θ_i does not depend on x. In other words, the spin configuration is composed of ferromagnetically ordered chains running in the x direction, with the interchain and intrachain distances given by $1/\sqrt{2}$ and $\sqrt{2}$, respectively. It is then convenient to Fourier-transform the fermion operators in the x direction only, according to

$$d_\alpha(x,y) = \left(\frac{2}{N}\right)^{1/4} \sum_{k_x} e^{ik_x x/\sqrt{2}} d_\alpha(k_x,y), \quad |k_x| < \pi. \quad (11)$$

Then the first two terms in Eq. (9) can be rewritten in the form

$$\tilde{\mathcal{H}} = -\sum_{y,k_x,\alpha,\beta} \cos\frac{k_x}{2} \left[t^{\alpha\beta}\left(y, y+\frac{1}{\sqrt{2}}\right) d_\alpha^\dagger(k_x,y) d_\beta\left(k_x, y\right. \right.$$

$$\left. \left. + \frac{1}{\sqrt{2}}\right) + \text{H.c.}\right] + \frac{J_H}{2} \sum_{y,k_x} [d_\downarrow^\dagger(k_x,y)d_\downarrow(k_x,y)$$

$$- d_\uparrow^\dagger(k_x,y)d_\uparrow(k_x,y)], \quad (12)$$

which we will also use in Sec. III below.

In the ferromagnetic state, the subsequent Fourier transformation in the y direction according to

$$d_\alpha(k_x,y) = \left(\frac{1}{2N}\right)^{1/4} \sum_{k_y} e^{ik_y y\sqrt{2}} d_{\vec{k}\alpha}, \quad |k_y| < \pi, \quad (13)$$

yields the spectrum

$$\epsilon_{\vec{k}}^{\uparrow,\downarrow} = \mp\frac{J_H}{2} + \epsilon_{\vec{k}}, \quad \epsilon_{\vec{k}} = -2\cos\frac{k_x}{2}\cos k_y. \quad (14)$$

The variation of spin direction within a Bloch wall corresponds to the long-wavelength limit $l_B \gg 1$ of continuum micromagnetic theory. Then one can define $\theta(y)$ as a continuous function, and the angle formed by the spins $\vec{S}(x,y)$ and $\vec{S}(x',y+1/\sqrt{2})$ on the neighboring chains is given by $(\partial\theta/\partial y)/\sqrt{2}$. For the case of a constant value of $\partial\theta/\partial y \ll 1$, the spin-up fermion spectrum $\tilde{\epsilon}_{\vec{k}}^\uparrow = -(J_H/2) + \tilde{\epsilon}_{\vec{k}}$ is obtained from Eqs. (10)–(12) [upon Fourier transformation, Eq. (13)]. When $\partial\theta/\partial y \neq 0$, the quantity $\tilde{\epsilon}_{\vec{k}}$ is only approximately factorizable,

$$\tilde{\epsilon}_{\vec{k}} = \cos\frac{k_x}{2} \left[\epsilon_y(k_y) + \delta\epsilon_y(k_x,k_y)\right], \quad \epsilon_y = -2\cos k_y,$$

$$\delta\epsilon_y = (\partial\theta/\partial y)^2 \left(\cos k_y - \frac{4}{J_H}\cos\frac{k_x}{2}\sin^2 k_y\right)\bigg/ 8. \quad (15)$$

The value of the carrier density at a fixed value of the chemical potential is then given by[25]

$$n = x + \delta x = \int_{-\mu/2}^{1} \frac{2d\epsilon_x}{\pi\sqrt{1-\epsilon_x^2}} \int_{-2}^{\mu/\epsilon_x} \{\rho_y(\epsilon_y)$$

$$+ \delta\rho_y(\epsilon_x,\epsilon_y)\} d\epsilon_y. \quad (16)$$

Here, $\rho_y = 1/(\pi\sqrt{4-\epsilon_y^2})$ is the value of the density of states at fixed k_x in the ferromagnetic state, and $\delta\rho_y$ is the correction arising at $\partial\theta/\partial y \neq 0$. Then the change in the carrier density due to a nonzero value of $(\partial\theta/\partial y) \ll 1$ can be evaluated (to leading order in $\delta\epsilon_y$) as

$$\delta x = \int_{-\mu/2}^{1} \frac{2d\epsilon_x}{\pi\sqrt{1-\epsilon_x^2}} \delta n_y\left(\frac{\mu}{\epsilon_x}\right),$$

$$\delta n_y\left(\frac{\mu}{\epsilon_x}\right) \equiv \int_{-2}^{\mu/\epsilon_x} \delta\rho_y(\epsilon_x,\epsilon_y) d\epsilon_y \approx -\delta\epsilon_y\rho_y\left(\frac{\mu}{\epsilon_x}\right). \quad (17)$$

Using Eq. (15), we obtain after some algebra

$$\delta x = \frac{\mathcal{C}}{2}\left(\frac{\partial\theta}{\partial y}\right)^2, \quad \mathcal{C} = \frac{1}{2\pi^2}\left[\left(\frac{\mu}{4} - \frac{\mu^2}{2J_H}\right)Y_1(x) + \frac{2}{J_H}Y_2(x)\right]. \quad (18)$$

Finally, given the known profile of $\theta(y)$ in a Bloch wall,[14] $\cos\theta(y) = \tanh(y/l_B)$, we find the following expression for the charge of a Bloch wall per unit length:

$$\sigma_B = -e\mathcal{C}/l_B, \quad (19)$$

where e is the absolute value of electron charge. In evaluating σ_B as $-e\int\delta x\,dy$, we used the adiabatic approximation, which is valid in the long-wavelength limit of $l_B \gg 1$. As expected, a similar calculation for a Bloch wall running parallel to a lattice direction yields the same result (19): Bloch walls have a well-defined continuum limit, and both their energy[26] and charge are independent of the orientation on a square lattice.

We note that at $J \gtrsim 0$, the Bloch wall can be stable only as long as the chemical potential at the center of the wall (where the band-narrowing effect is most pronounced) lies above the bottom of the carrier band. In other words, the value of $x + \delta x$ with δx given by Eq. (18) should remain positive at $y = 0$ (otherwise, there would be no carriers and hence no carrier-mediated ferromagnetic interaction near the center of the wall).[27] Since the wall is smooth, $l_B \gg 1$, this condition is important only at the low-doping limit of $x \ll 1$, when it reads[28]

$$16\pi x DS > K. \quad (20)$$

This is clearly violated at sufficiently low x. We will see that in this case the domain wall is in fact abrupt [Sec. III, Eq. (21)].

According to Eq. (19), the charge of the Bloch wall, which is inversely proportional to its width, decreases with decreasing anisotropy strength: $\sigma_B \propto \sqrt{K}$. At small values of electron density, $x \ll 1, J_H$, we find $\sigma_B = e/(8\pi l_B)$. The behavior of σ_B at the intermediate doping levels can be inferred from Fig. 1(b), where the quantity $\mathcal{C}(x)$ [see Eqs. (18) and (19)] is plotted for different values of J_H. We suggest that the experimental determination of σ_B may help to distinguish Bloch walls from abrupt or stripe domain walls (see Secs. III and IV below), which typically carry larger charge. On the theory side, the effect of Bloch wall charge on the carrier transport across the wall should be considered.
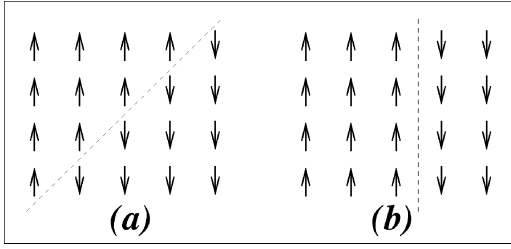
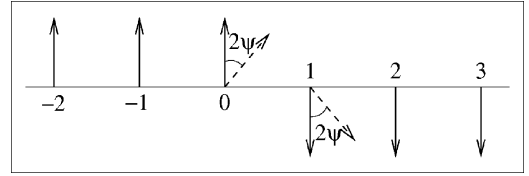FIG. 2. Diagonal (a) and vertical (b) abrupt domain walls (dashed lines).

FIG. 3. Schematic representation of a one-dimensional problem which arises in diagonal domain wall calculations, Eqs. (23) and (24). The intersite distance is equal to $1/\sqrt{2}$, and the numbers are the same as the subscripts of the fermion operators in Eq. (24). Dashed arrows correspond to the perturbed case, $\psi \neq 0$.

Throughout this section, we assumed[29] that the Debye-Hückel screening radius is large in comparison to l_B. This appears to be plausible, especially in view of the relatively large values of dielectric constants, characteristic of the highly polarizable oxides. We will briefly discuss the magnitude of the Coulomb correction to the Bloch wall energy, S_B, in Appendix B [Eq. (B9)]. In the opposite case of strong screening, the charge of a Bloch wall will vanish.

III. ABRUPT WALL

The appreciable contribution of magnetic domain walls to resistivity, as observed in certain ferromagnetic strained CMR films,[5–7] suggests the possibility of non-Bloch walls arising in these systems. Indeed, in order to scatter the carriers effectively the domain wall must have a nonsmooth structure, characterized by abrupt changes in the spin direction. An abrupt (Ising-type) domain wall, shown in Fig. 2, represents an extreme example of such a structure.

Unlike the Bloch wall, an abrupt wall represents a lattice problem (as opposed to a long-wavelength one). Therefore the properties of an abrupt wall depend on its orientation with respect to the lattice, and one has to distinguish between, e.g., diagonal [Fig. 2(a)] and vertical [Fig. 2(b)] walls. We note that a similar feature would also arise for domain walls in an Ising ferromagnet—indeed, the number of cut ferromagnetic links per unit wall length is different for vertical and diagonal walls. In a classical double-exchange ferromagnet, the standard double-exchange mechanism forbids carrier hopping across the abrupt domain wall.[30] Owing to the anisotropy of the carrier spectrum (as manifested in a nonspherical shape of the Fermi surface), the carrier contribution to the abrupt wall energy is again orientation dependent.

In order to show that abrupt domain walls can actually arise in double-exchange ferromagnets, we will first turn to the low-doping limit $x \ll 1$, assuming also that $J_H = \infty$ and $J = 0$. Since the Fermi momentum is small, $p_F^2 = 4\pi x \ll 1$, carrier dispersion can be approximated by the free-particle dispersion law $\epsilon_k^\uparrow \approx \text{const} + (k^2/2)$. The energy of an abrupt wall is therefore equal to that of a partition inserted into an ideal spin-polarized Fermi gas, which can be easily estimated.

Let the ideal Fermi gas be contained in a rectangular box of size $L_x \times L_y$. According to the uncertainty principle (or

alternatively to the usual rules of momentum quantization), the difference between the allowed values $p_y^{(i)}$ of the y component of momentum can be estimated as $\delta p_y \sim 1/L_y$. Suppose now that a flat partition perpendicular to the y axis has been introduced, dividing the box in half. This shifts each allowed momentum value: $p_y^{(i)} \rightarrow p_y^{(i)} + \delta p_y^{(i)}$ with $|\delta p_y^{(i)}| \sim \delta p_y$. The signs of $\delta p_y^{(i)}$ are chosen in such a way that the *energy* shift of each individual electron level is positive: $\delta \epsilon(p_x, p_y) \sim |p_y| \delta p_y$. The net energy change associated with the partition is thus given by $L_x L_y \int n_{\vec{p}} |p_y| d^2 p / L_y$, or $\sim x^{3/2}$ per unit length of partition.[31]

Thus, we find that the energy of abrupt domain wall in a double-exchange ferromagnet is given by $S_A \sim x^{3/2}$. The numerical coefficient can be obtained by an exact treatment [see below and Appendix A, Eqs. (A16) and (A17)], yielding $S_A \approx 4\sqrt{\pi} x^{3/2}/3$. Comparing this with the Bloch wall energy $S_B \approx \sqrt{Kx}$ [see Eq. (2)], we find that the abrupt wall energy is lower, $S_A < S_B$, as long as

$$x^2 < 9K/16\pi. \qquad (21)$$

We note that according to Eq. (20), Bloch walls become altogether unstable at $x^2 < K/4\pi$.

It appears to be very difficult to rigorously address the question whether in the region specified by inequality (21) the abrupt wall actually represents the optimal spin configuration. We are, however, able to verify [see Appendix A, Eqs. (A16) and (A17)] that as long as $x^2 < K/\pi$, the abrupt domain wall is stable with respect to small "smearing" perturbations (shown schematically in Fig. 3) involving spins adjacent to the domain wall on both sides. This provides a strong, albeit variational, argument for the overall stability of abrupt walls.

We now turn to an exact calculation of the energies and charges of abrupt walls for all values of x, J_H, and J, beginning with the evaluation of the electronic contribution to the energy of an abrupt diagonal wall.

Following the Fourier transform, Eq. (11), the electronic terms in the Hamiltonian of the uniform ferromagnetic phase take the form [cf. Eq. (12)]

$$\tilde{\mathcal{H}} = \sum_{k_x} \mathcal{H}_{k_x}, \tag{22}$$

$$\mathcal{H}_{k_x} = -\frac{Q}{2} \sum_y \left\{ d_\uparrow^\dagger\left(k_x, y + \frac{1}{\sqrt{2}}\right) d_\uparrow(k_x, y) \right.$$

$$+ d_\downarrow^\dagger\left(k_x, y + \frac{1}{\sqrt{2}}\right) d_\downarrow(k_x, y) + \text{H.c.} \Big\}$$

$$+ \frac{J_H}{2} \sum_y \{ d_\downarrow^\dagger(k_x, y) d_\downarrow(k_x, y) - d_\uparrow^\dagger(k_x, y) d_\uparrow(k_x, y) \}, \tag{23}$$

where $Q = 2\cos(k_x/2)$. The abrupt diagonal domain wall parallel to the x axis results in a perturbation of the Hamiltonian (23), $\mathcal{H}_{k_x} \to \mathcal{H}_{k_x} + V_{k_x}$, with

$$\frac{2}{Q} V_{k_x} = \{ d_{-1\uparrow}^\dagger d_{0\uparrow} + d_{-1\downarrow}^\dagger d_{0\downarrow} + d_{1\uparrow}^\dagger d_{2\uparrow} + d_{1\downarrow}^\dagger d_{2\downarrow} \}(1 - \cos\psi)$$

$$+ \{ d_{0\uparrow}^\dagger d_{1\uparrow} + d_{0\downarrow}^\dagger d_{1\downarrow} \}(1 - \sin 2\psi)$$

$$+ \{ d_{0\uparrow}^\dagger d_{1\downarrow} - d_{0\downarrow}^\dagger d_{1\uparrow} \}\cos 2\psi + \{ d_{-1\uparrow}^\dagger d_{0\downarrow} - d_{-1\downarrow}^\dagger d_{0\uparrow} $$

$$+ d_{1\uparrow}^\dagger d_{2\downarrow} - d_{1\downarrow}^\dagger d_{2\uparrow} \}\sin\psi + \text{H.c.} \tag{24}$$

Here we denoted $d_\alpha(k_x, i/\sqrt{2})$ by $d_{i\alpha}$ and allowed for a smearing perturbation, $\psi \ll 1$, as shown in Fig. 3. It is convenient to rewrite the operator V_{k_x} in a diagonal form:

$$V_{k_x} = \sum_{i=1}^{8} A_i a_i^\dagger a_i, \quad a_i^\dagger a_j + a_j a_i^\dagger = \delta_{ij}. \tag{25}$$

Expressions for both the eigenvalues A_i and the operators a_i are given in Appendix A.

In the absence of a domain wall, the electronic contribution to the thermodynamic potential of a double-exchange ferromagnet at a temperature T can be evaluated as

$$\Omega = \int \frac{L_x dk_x}{2\pi\sqrt{2}} \int \frac{L_y \sqrt{2} dk_y}{2\pi} \varphi[\epsilon_{\vec{k}}]$$

$$= \int \frac{L_x dk_x}{2\pi\sqrt{2}} \int d\epsilon\, \nu_{tot}(\epsilon, Q) \varphi(\epsilon) d\epsilon,$$

$$\epsilon_{\vec{k}} = -Q\cos k_y, \quad \varphi(\epsilon) = -T \ln\left[1 + \exp\left(\frac{\mu - \epsilon}{T}\right)\right]. \tag{26}$$

Here, L_x and L_y are the dimensions of the sample, $\nu_{tot}(\epsilon, Q) = L_y \sqrt{2}/(\pi\sqrt{Q^2 - \epsilon^2})$ is the total density of states at a fixed value of Q [i.e., with $k_x = \pm 2\arccos(Q/2)$], and the factors $\sqrt{2}$ originate in momentum rescaling implied in Eqs. (11) and (13).

When the domain wall perpendicular to the y axis is introduced, the associated perturbation V_{k_x}, Eqs. (24) and (25), gives rise to a correction[32] in the density of states, $\nu_{tot}(\epsilon, Q) \to \nu_{tot}(\epsilon, Q) + \delta\nu(\epsilon, Q)$. Introducing the Lifshits-

Krein spectral shift function[33] $\xi(\epsilon, Q)$ according to $\delta\nu = -\partial\xi/\partial\epsilon$, we find, for the electronic contribution to the domain wall energy,

$$\frac{\delta\Omega}{L_x} = \int \frac{dk_x}{2\pi\sqrt{2}} \int d\epsilon\, \delta\nu(\epsilon, Q) \varphi(\epsilon)$$

$$= \int \frac{dk_x}{2\pi\sqrt{2}} \int d\epsilon\, \xi(\epsilon, Q) f(\epsilon). \tag{27}$$

Here, the zero-temperature value for the Fermi distribution function $f(\epsilon) = \theta(\mu - \epsilon)$ can be substituted.

For a given value of k_x, the operator V_{k_x} represents a local perturbation of a one-dimensional Hamiltonian $\mathcal{H}_{k_x}$. Thus, the dependence of ξ on Q is only parametric,[32] and the value of ξ can be found from the standard formula[33] (see also Ref. 34)

$$\xi(\epsilon, Q(k_x)) = -\frac{1}{\pi} \text{Arg Det}\left[\hat{I} - \hat{G}\left(\epsilon - \frac{1}{2}J_H - i0, Q\right) V_{k_x} \right], \tag{28}$$

where $\hat{G}(\zeta, Q) = (\zeta \cdot \hat{I} - \mathcal{H}_{k_x})^{-1}$ is the resolvent operator at a given value of k_x, and $\hat{I}$ is the identity operator. In the basis containing the states $a_i^\dagger|0\rangle$ (where $|0\rangle$ is the vacuum state), the determinant on the right-hand side (RHS) of Eq. (28) is that of an 8×8 matrix, $\delta_{ij} - M_{ij}A_j$, with

$$M_{ij} = \sum_{\alpha=\uparrow,\downarrow} \int \frac{dk_y \sqrt{2}}{2\pi Q} \frac{\langle 0|a_i|k_y^\alpha\rangle\langle k_y^\alpha|a_j^\dagger|0\rangle}{E_\alpha + \cos k_y - i0}. \tag{29}$$

Here

$$E_\uparrow = \epsilon/Q, \quad E_\downarrow = (\epsilon - J_H)/Q, \tag{30}$$

and $|k_y^\alpha\rangle$ are properly normalized Bloch wave states,

$$|k_y^\alpha\rangle = \frac{1}{2^{1/4}} \sum_y e^{-ik_y y\sqrt{2}} d_\alpha^\dagger(k_x, y)|0\rangle,$$

$$\langle k_y^\alpha | k_y'^\beta \rangle = 2\pi\delta(k_y - k_y')\delta_{\alpha\beta}. \tag{31}$$

After a straightforward, if somewhat laborious, calculation we obtain

$$\xi(\epsilon, Q) = \xi^{(0)}(\epsilon, Q) + \delta\xi, \quad \tan\pi\xi^{(0)} = \frac{E_\uparrow E_\downarrow - 1}{\sqrt{E_\downarrow^2 - 1}\sqrt{1 - E_\uparrow^2}},$$

$$\delta\xi = \frac{4J_H^2}{\pi Q^2} \sqrt{1 - E_\uparrow^2} \frac{E_\uparrow - E_\downarrow - \sqrt{E_\downarrow^2 - 1}}{E_\downarrow^2 - E_\uparrow^2 - 2E_\uparrow E_\downarrow} \psi^2. \tag{32}$$

The final expression for the energy of an abrupt diagonal domain wall per unit length is then given by the trace formula, Eq. (27), with additional contributions from direct superexchange and single-ion anisotropy:

$$S_d \equiv S_d^{(0)} + Z_d \psi^2 = -2\sqrt{2}J + 2\sqrt{2}(2J+K)\psi^2$$

$$+ \frac{\sqrt{2}}{\pi} \int_{-1}^{1} dE_\uparrow \int_0^2 \frac{Q \, dQ}{\sqrt{4-Q^2}} \, \xi(QE_\uparrow, Q) \theta(\mu - QE_\uparrow).$$

$$(33)$$

The energy of a vertical abrupt domain wall is calculated very similarly (see Appendix A), yielding the result

$$S_v \equiv S_v^{(0)} + Z_v \psi^2 = -2J + 4(J+K)\psi^2$$

$$+ \frac{1}{\pi} \int_{-1}^{1} \frac{d\epsilon_1}{\sqrt{1-\epsilon_1^2}} \int_{-1}^{1} d\epsilon_2 \tilde{\xi}(\epsilon_2) \theta(\mu - \epsilon_1 - \epsilon_2).$$

$$(34)$$

Here, $\tilde{\xi}(\epsilon_2)$ is equal to $\xi(\epsilon_2, Q)$ as given by Eqs. (32) with $E_\uparrow = \epsilon_2$, $E_\downarrow = \epsilon_2 - J_H$, and $Q=1$.

The spectral shift function, Eq. (32), also contains information about the abrupt domain wall charges. Indeed, the spectral shift function $\xi(\epsilon)$ generally measures the number of energy levels that cross the given energy value ϵ as a result of a perturbation. Thus, the change in electron density at a fixed value of k_x is given by $-\xi(\mu, Q)$, yielding the charge of an unperturbed ($\psi = 0$) abrupt diagonal wall:

$$\sigma_d = \frac{\sqrt{2}}{\pi} e \int_{|\mu|}^{2} \xi^{(0)}\left(\frac{\mu}{Q}, Q\right) \frac{dQ}{\sqrt{4-Q^2}}. \qquad (35)$$

For a vertical wall, we likewise obtain

$$\sigma_v = \frac{e}{\pi} \int_{|\mu|-1}^{1} \tilde{\xi}^{(0)}(\mu - \epsilon_1 \operatorname{sgn} \mu) \frac{d\epsilon_1}{\sqrt{1-\epsilon_1^2}}. \qquad (36)$$

Here the function $\tilde{\xi}(\epsilon)$ is defined in the same way as in Eq. (34) above.

We have conducted a thorough numerical investigation of Eqs. (33) and (34). The doping dependence of the abrupt wall energies for different values of J_H is illustrated in Fig. 4(a). Comparing these with Fig. 1(a), we conclude that at the intermediate doping levels, abrupt wall energies are typically several times larger than the spin stiffness, DS. Therefore in the physically relevant case of small anisotropies, $K \ll DS$, Bloch walls will typically have a significantly lower energy [see Eq. (2)]. We note that including antiferromagnetic superexchange, $J > 0$, would lead to a decrease in $S_d^{(0)}$ relative to $S_v^{(0)}$ [as follows from Eqs. (33) and (34)]. In particular, this can yield[35] $S_d^{(0)} < S_v^{(0)}$ at small values of x.

The charges σ_d and σ_v of the abrupt domain walls are plotted in Fig. 4(b). We see that at the intermediate doping values, the electric charge per unit length is of the order of $0.1e$, in a marked difference from weakly charged Bloch walls [cf. Fig. 1 and Eq. (19)].

With increasing antiferromagnetic interactions in the system (that is, either with increasing J or with decreasing J_H) the spin stiffness, as well as the abrupt wall energies, will eventually change sign. Near this point, there might be a region where DS is still positive, while either $S_v^{(0)}$ or $S_d^{(0)}$ is smaller than the Bloch wall energy S_B. This is due to the
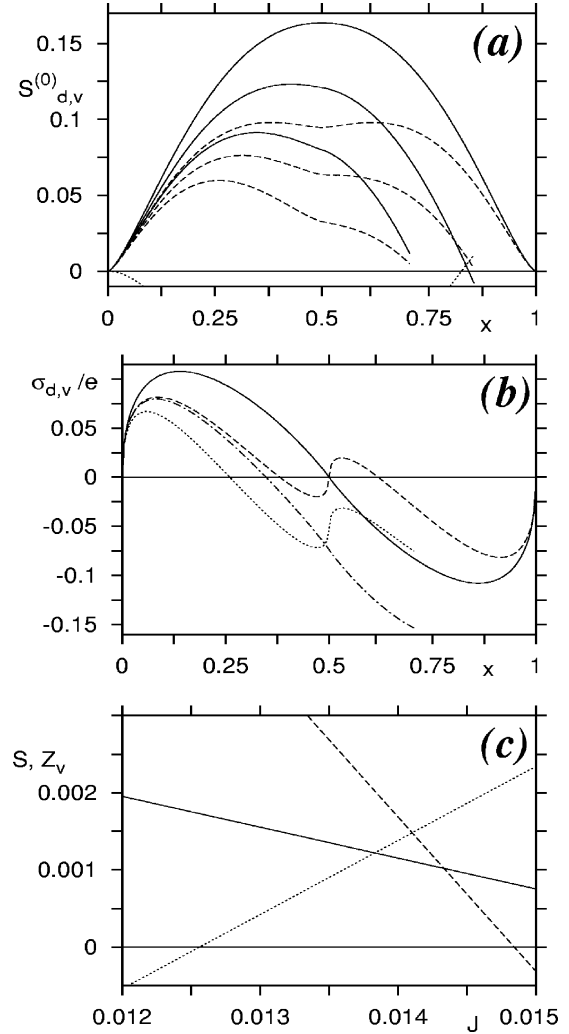

FIG. 4. (a) Abrupt wall energies vs x at $J=0$. Solid (dashed) lines, top to bottom: diagonal wall energy $S_d^{(0)}$ (vertical wall energy $S_v^{(0)}$) for $J_H \to \infty$, $J_H = 8$, and $J_H = 4$. For finite values of J_H, the lines end at the values of x corresponding to the sign change of spin stiffness D. Immediately below these values, the ferromagnetic state is unstable with respect to phase separation (see Fig. 1). For $K(x) = D(x)S/25$ (i.e., $l_B = 5$), the quantities $Z_{d,v}$ are negative everywhere outside the low-doping regions $x \ll 1$ and $1 - x \ll 1$, except for the case of $J_H = 8$, when Z_d becomes positive for $x > 0.83$ (dotted line). (b) Abrupt wall charges in units of electron charge $|e|$. Solid and dashed (dash-dotted and dotted) lines represent σ_d and σ_v for $J_H \to \infty$ ($J_H = 4$). (c) Bloch wall energy S_B (solid line), abrupt vertical wall energy $S_v^{(0)}$ (dashed line), and the quantity Z_v (dotted line) vs superexchange J. Anisotropy constant varies according to $K(J) = DS/25$. Conduction electron density and Hund's rule coupling strength are given by $x = 0.55$ and $J_H = 4$, respectively, and the system is unstable with respect to phase separation.

fact that S_B and $S_{v,d}^{(0)}$ depend on J and J_H in different ways. Such a situation is illustrated in Fig. 4(c), showing the domain wall energies in a double-exchange ferromagnet with $x = 0.55$ and $J_H = 4$ as functions of J. The solid line corresponds to the Bloch wall energy S_B, whereas the vertical abrupt wall energy $S_v^{(0)}$ is represented by a dashed line. The value of the easy-axis anisotropy constant K is varied with J
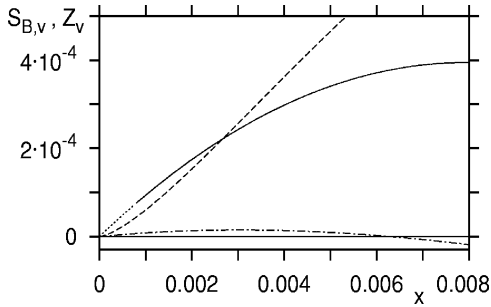
FIG. 5. Bloch wall energy S_B (solid line), abrupt vertical wall energy $S_v^{(0)}$ (dashed line), and the quantity Z_v (dash-dotted line) vs electron density x in the low-density limit without superexchange ($J=0$). Hund's rule coupling is fixed at $J_H=0.1$, while the anisotropy varies according to $K(x)=DS/25$, leading to a constant Bloch wall width $l_B=5$. The Bloch wall, however, becomes unstable at lower x (dotted line).

in such a way that the Bloch wall width l_B [see Eq. (2)] is always equal to 5. We see that $S_B>S_v^{(0)}>0$ for $0.0143<J<0.0148$. Since the quantity Z_v [see Eq. (34)], represented by the dotted line, is positive throughout the $S_v^{(0)}<S_B$ region, one is tempted to conclude that the abrupt wall is indeed stable in this region. However, it is easy to verify that for $J>0.0107$, the homogeneous ferromagnetic ground state becomes unstable with respect to phase separation into ferro- and antiferromagnetic regions. It appears that this represents the general situation, i.e., that at the intermediate doping range the inequality $S_B>S_v^{(0)}$ (or $S_B>S_d^{(0)}$) cannot be satisfied within the thermodynamically stable region. In Sec. IV below, we will argue that the phenomenon of phase separation can affect the magnetic domain wall structure in a profound way. Here we merely note that even if phase separation is suppressed due to some mechanism (e.g., enforcing electric neutrality on the microscopic level), the parameter region where either S_v or S_d is smaller than S_B (but the stiffness D is still positive) would still be very narrow, requiring one to fine-tune the values of J, J_H, K, and x to within a fraction of a percent.[36] It is therefore very unlikely that such a situation can be realized experimentally in a reproducible way.

Expressions (33)–(36) can be further simplified in the limiting cases of small carrier density, $x\ll1$, or large Hund's rule coupling, $J_H\rightarrow\infty$ (see Appendix A). Expressions (A12)–(A15), valid in the $J_H\rightarrow\infty$ limit, can be used to estimate the values of S_d and S_v at sufficiently large J_H throughout the entire range of dopant concentrations.

As discussed in the beginning of this section [see Eq. (21)], the domain walls become abrupt at the low-doping limit of $x\ll1$. In this case, the abrupt wall energies and charges are given by Eqs. (A16)–(A19). The doping dependence of domain wall energies in this region is illustrated in Fig. 5. The value of Hund's rule coupling is taken to be $J_H=0.1$, and $K(x)=D(x)S/25$, again ensuring that $l_B=5$. We see that the energy of an abrupt vertical wall (dashed line) is lower than that of a Bloch wall (solid line), $S_v^{(0)}<S_B$, for all $x<0.0027$, and the stability of abrupt domain wall is further evidenced by the fact that the quantity Z_v (dash-dotted line)

is positive for $x<0.0063$. For this choice of parameters,[37] the value of $S_d^{(0)}$ is just above that of $S_v^{(0)}$, and we find $S_d^{(0)}<S_B$ at $x<0.0026$ and $Z_d>0$ for all $x<0.0074$. The Bloch wall becomes unstable [see Eq. (20)] at $x<0.0008$ (dotted line). We note that allowing for a larger value of K would have broadened the region where abrupt walls have lower energy; however, Eqs. (2) are valid only in the $l_B\gg1$ case.

The data shown in Fig. 5 are for a system with no direct superexchange, $J=0$; including a small $J>0$ would give rise to a phase-separation instability at small x,[22] which may or may not cover the entire region of $S_{v,d}^{(0)}<S_B$. While no study of domain structure in the electron-doped manganates has been reported so far, it appears that superexchange in these systems is sufficiently strong to destabilize the homogeneous ferromagnetic state at $x\ll1$.[38] The abrupt wall picture as discussed here is then inapplicable (see Sec. IV below). We note, however, that this might not be the case for other lightly doped magnetic semiconductors or semimetals. Ferromagnetic semiconductors such as Eu-doped EuS and EuO have relatively high values of the Curie temperature T_C (Ref. 39), presumably originating from a strong ferromagnetic superexchange, $J<0$. In this case, even in a lightly doped sample ferromagnetism is due mostly to superexchange (rather than to double exchange) and one expects that the domain walls will be of Bloch type, like in conventional Heisenberg ferromagnets. However, other magnetic semiconductors such as EuSe become ferromagnetic only upon small electron doping.[40] In this case of small positive J, domain walls may in fact be abrupt. This also may be the case in a ferromagnetic semimetal EuB$_6$ (Ref. 41). It would therefore be most interesting to study experimentally the domain wall structure (in particular, the effect of domain walls on the transport properties) in the ferromagnetic films of these compounds.

Throughout our calculation, we neglected the effects of chemical disorder which can lead to localization of electron states. We note that the overall profile of carrier wave functions does not directly affect the properties of an abrupt wall. The assumption essential for our approach is that the electron wave function can be *locally* approximated by an energy eigenfunction of the clean case[42] with the same energy. This is valid provided that the localization length is much larger than the inverse Fermi momentum; the latter condition is expected to be satisfied in manganates within the metallic regime, as well as in the doped magnetic semiconductors and semimetals discussed above.

IV. PHASE SEPARATION AND STRIPE WALLS

Phase separation is a phenomenon which commonly occurs in the CMR manganese oxides.[20,21] Although direct evidence is lacking, it appears likely that the films studied in Refs. 5–7 are in fact phase separated. It is therefore important to consider the effect of phase separation on magnetic domain wall structure in double-exchange ferromagnets.

Let us first suppose that the values of the parameters of the system (that is, carrier density x, superexchange J, Hund's rule coupling strength J_H) lie within the stability region of the uniform ferromagnetic phase. The thermody-

namic potential is then given by $\Omega_{FM} = E + 2J - \mu x$, with the value of $\mu = \mu_{FM}(x)$ determined by the uniform conduction electron density x. The electron charge density $-ex$ is compensated by the combined charge of magnetic and non-magnetic ions, resulting in electric neutrality of the system on the microscopic level.[43] As the values of parameters are varied (e.g., either the value of J is increased or that of J_H is decreased), the system eventually becomes unstable with respect to phase separation into the ferromagnetic phase and another phase which we will call antiferromagnetic.[44] In the absence of a Coulomb interaction, this occurs when the thermodynamic potentials of the two phases become equal to each other: $\Omega_{FM}(\mu_{FM}(x)) = \Omega_{AFM}(\mu_{FM}(x))$. At this point, it becomes energetically advantageous to create islands of the antiferromagnetic phase within the bulk of the ferromagnet. Since there is a finite energy cost W associated with a unit length of the boundary between the two phases, such an island should contain a large number of sites in order to reduce the boundary energy per antiferromagnetic site; as long as this is the case, the area occupied by the antiferromagnetic phase can be arbitrarily small relative to the total size of the system, so that the carrier density x within the ferromagnetic area and hence the value of chemical potential $\mu_{FM}(x)$ remain unchanged.

The structure of the boundaries between different phases has been studied by the present writer in Ref. 22. It was found that at least in some cases these boundaries are abrupt; it appears plausible that this property is rather generic. We note that the energy and charge of an abrupt interphase boundary can be evaluated using the approach applied in Sec. III above to the study of an abrupt domain wall. A boundary between ferro- and antiferromagnetic areas can be perfectly abrupt only if it runs parallel to certain lattice directions.[22] It is therefore likely that within a large region of parameter values, the emerging islands of the antiferromagnetic phase will have a square (or diamond) shape. Apart from one case discussed towards the end of this section, the latter feature is unimportant for the rather qualitative discussion below. We will therefore assume that the islands are circular, which would correspond to the boundary energy W independent of direction.

While the chemical potential $\mu = \mu_{FM}(x)$ is constant across the sample, the carrier density within the island, x_{AFM}, is different from the nominal value x. We note that phase separation consists precisely in a redistribution of the carriers with a simultaneous change in magnetic ordering, and would not be possible had the requirement of constant carrier density been enforced on the microscopic level. The island is therefore electrically charged, and it is imperative to take into account the effects of electrostatic Coulomb interaction and screening on phase separation.

In a thin film, the inverse Debye-Hückel screening radius is given by[45,46] (see also Appendix B):

$$\kappa = \frac{2\pi e^2 \nu_0}{\bar{\epsilon}}, \quad \bar{\epsilon} = \frac{1}{2}(\epsilon_{d1} + \epsilon_{d2}). \tag{37}$$

Here ν_0 is the value of the carrier density of states at the Fermi level and ϵ_{d1}, ϵ_{d2} are dielectric constants of the media

on both sides of the conducting layer. In the 3D case, which is discussed in more detail in Appendix B, $\kappa_{(3D)}^2 = 4\pi e^2 \nu_0 / \epsilon_d$, where ϵ_d is the dielectric constant of the double-exchange magnet itself. If the size of the island was large in comparison with the Debye-Hückel radius, $R \gg \kappa^{-1}$, screening within the island would have restored the carrier density to its nominal value x (and charge density to zero). In the case when there is no conduction band in the bulk antiferromagnetic phase [e.g., when $x_{AFM}(\mu)$ equals either 0 or 1], the presence of the electric potential φ (which in this case is strongly position dependent) would shift the carrier band within the island either upwards or downwards. This in turn will ultimately give rise to a Fermi surface, screening, and restoration of the carrier density to its nominal value on the length scale of κ^{-1}. However, as explained above, when the value of the density is fixed no phase separation is possible. We therefore conclude that the formation of an island can be energetically favorable only as long as[47] $R \lesssim \kappa^{-1}$. We will assume for simplicity that $1 \ll R \ll \kappa^{-1}$, that is, that the carrier density within the island is uniform and equal to the bulk value of $x_{AFM}(\mu)$. This obviously includes an assumption that Debye-Hückel radius is large on the atomic length scale, $\kappa \ll 1$. The latter is not unphysical, in view of the relatively large dielectric constants ϵ_d reported for the manganates[48] and of the suppression of the carrier density of states at the Fermi level ν_0 found in the x-ray absorption and angle-resolved photoemission measurements.[49] For a thin film, the situation also depends on the choice of substrate, as discussed in more detail at the end of this section.

With these assumptions, the change in the thermodynamic potential Ω associated with the creation of a single circular antiferromagnetic island in a 2D system can be evaluated as[50]

$$X_i = \pi R^2 (\Omega_{AFM} - \Omega_{FM}) + 2\pi R W + \frac{1}{2} \int d^2 r \rho(\vec{r}) \varphi(\vec{r})$$

$$+ \int_{(FM)} d^2 r \int_\mu^{\mu'} d\epsilon (\epsilon - \mu) \nu_0. \tag{38}$$

Here, the first two terms represent the bulk and boundary contributions, the third term is the electrostatic Coulomb energy, and the last term is the kinetic energy cost of redistributing electrons in the ferromagnet, caused by a shift of the electrochemical potential $\mu'(\vec{r}) = \mu + e\varphi(\vec{r})$ (that is, a shift of the band energies due to the presence of an electric field within the screening cloud). The charge density $\rho(r)$ equals $\rho_{AFM} = -e(x_{AFM} - x)$ within the island and $-e\,\delta x(\vec{r})$ outside, where δx is the change of electron density in the screening cloud. The last term in Eq. (38) can be rewritten as

$$\frac{1}{2} \int_{(FM)} d^2 r \frac{(\delta x)^2}{\nu_0} = \frac{1}{2} \int_{(FM)} e\varphi \,\delta x \, d^2 r = -\frac{1}{2} \int_{(FM)} \rho \varphi \, d^2 r.$$

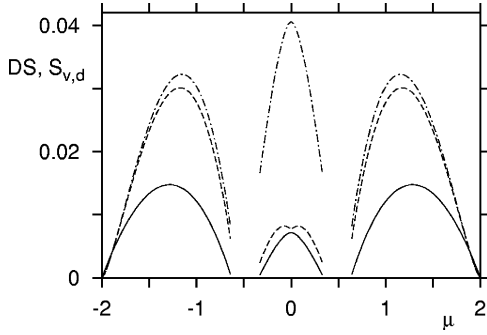This allows us to render Eq. (38) in the form

FIG. 6. Chemical potential dependence of spin stiffness DS (solid line) and the diagonal and vertical abrupt domain wall energies (dash-dotted and dashed lines) for a $J_H \to \infty$ system on the brink of phase separation. The value of J is adjusted in such a way that $\Omega_{FM} = \Omega_{AFM}$ for any value of carrier density x. The nature of the corresponding antiferromagnetic phases is discussed in the text.

$$X_i = \pi R^2 (\Omega_{AFM} - \Omega_{FM}) + 2\pi RW + \frac{1}{2} \int_{(AFM)} d^2 r \rho \varphi, \quad (39)$$

where the integration in the last term is carried out over the area of the island. Evaluating the potential φ to leading order in $1/(\kappa R) \ll 1$ [see Appendix B, Eqs. (B11) and (B12)], we obtain

$$X_i = \pi R^2 (\Omega_{AFM} - \Omega_{FM}) + 2\pi RW + \frac{8\pi \rho_{AFM}^2 R^3}{3\bar{\epsilon}}. \quad (40)$$

The creation of an island becomes energetically favorable once the minimum value of this expression drops below zero. This yields the following threshold condition for phase separation to occur:

$$\Omega_{FM} - \Omega_{AFM} > \Delta_0 = 8 |\rho_{AFM}| \sqrt{\frac{W}{3\bar{\epsilon}}} \quad (41)$$

[at $\Omega_{FM} = \Omega_{AFM} + \Delta_0$, the discriminant of the cubic equation $X_i(R) = 0$ vanishes; the minimum value $X_i(R_0) = 0$ is then reached at $R_0 = (3\bar{\epsilon}W)^{1/2}/(2|\rho_{AFM}|)$].

Let us now consider a domain wall in a phase-separated film. We note that in this case the antiferromagnetic and ferromagnetic tendencies in the system are approximately balanced against each other; this greatly reduces both the spin stiffness [which in turn determines the Bloch wall energy via Eq. (2)] and the energy of abrupt domain walls, $S_{v,d}^{(0)}$. This point is illustrated by Fig. 6, representing the chemical potential dependence of spin stiffness (solid line) and abrupt wall energies (dashed and dash-dotted lines) for a $J_H \to \infty$ system with the value of $J = J(\mu)$ adjusted in such a way[51] that $\Omega_{FM} = \Omega_{AFM}$. The appropriate antiferromagnetic phase near the end points $\mu = \pm 2$ is characterized by the usual Néel $\{\pi, \pi\}$ (G-antiferromagnetic) spin ordering, whereas in the vicinity of quarter-filling, $\mu = 0$, the A-antiferromagnetic phase with the ordering vector $\{\pi, 0\}$ proves more advantageous. The plethora of possible phases arising in the intermediate case (see Ref. 22) are not considered here, and no

value is plotted for DS and $S_{v,d}^{(0)}$ unless the phase separation into the ferromagnetic and either G- or A-antiferromagnetic phases is possible. Comparing Fig. 6 with the $J = 0$ case, plotted in Figs. 1(a) and 4(a), we find a drastic reduction of both spin stiffness and domain wall energies at the intermediate doping values. In addition, the energies of abrupt domain walls are now of the same order of magnitude as the spin stiffness, in a marked difference with the single-phase case considered earlier.

We will first discuss the effect of Coulomb forces in the case when the value of $\Omega_{FM} - \Omega_{AFM}$ is just above the threshold, Eq. (41), so that the islands of the antiferromagnetic phase arising within each ferromagnetic domain are well separated from each other, and Eqs. (38)–(40) are valid. As discussed in Sec. III, the abrupt domain wall shuts the carrier hopping in the perpendicular direction, acting as a partition in the gas of conduction electrons. In the absence of Coulomb forces, the energy cost of creating a stripe of antiferromagnetic phase adjacent to the wall is therefore equal to $-(\Omega_{FM} - \Omega_{AFM})d$ (where d is the stripe width) per unit length of the stripe, and does not include any additional boundary contribution. This statement (which is equivalent to saying that the abrupt wall energy is equal to $2W$ per unit length) is exact in the $J_H \to \infty$ limit (see Appendix A and Fig. 10). It is also clear that it provides a reasonable estimate for the case of large but finite J_H; the details of the situation at finite J_H will be addressed elsewhere. Thus, when $\Omega_{FM} - \Omega_{AFM} > 0$, the energy of an abrupt domain wall can be further lowered by inserting alongside it a stripe of antiferromagnetic phase (see Fig. 7). The width of the stripe is determined by a trade-off between the bulk and Coulomb energies, i.e., by minimizing the energy of a *stripe domain wall* per unit length,
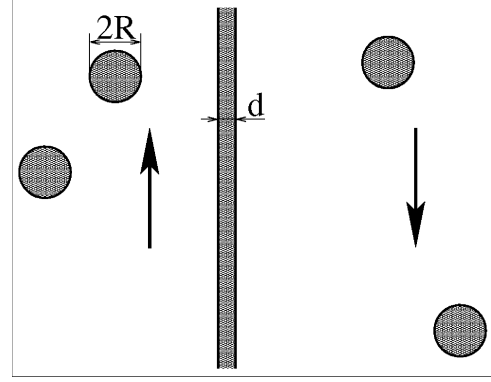

FIG. 7. Schematic representation of a stripe domain wall in a phase-separated double-exchange magnet. The two ferromagnetic domains with antiparallel directions of magnetization (arrows) are separated by a stripe of antiferromagnetic phase (shaded). In addition, unconnected islands of antiferromagnetic phase are formed within each domain.

$$S_s(d) = 2W - (\Omega_{FM} - \Omega_{AFM})d - \frac{d^2}{\bar{\epsilon}} \rho_{AFM}^2 \ln \kappa d \quad (42)$$

[see Appendix B, Eqs. (B6)–(B8)]. Since the antiferromagnetic stripe separates two ferromagnetic domains with anti-

parallel directions of magnetization, the spins at the two edges of the stripe must point in the opposite directions. For the stripe of an A antiferromagnet (G antiferromagnet) parallel to a lattice direction (lattice diagonal), this means that the number d (the number $\sqrt{2}d$) must be odd[52]; similar conditions should hold for other phases. Since we assumed that the value of d is sufficiently large, $d \gg 1$, these requirements do not affect our estimates. Assuming that $\Omega_{FM} - \Omega_{AFM} = \Delta\Omega_0$, we find

$$d_s = \frac{8\sqrt{\bar{\epsilon}W/3}}{\rho_{AFM}\ln\dfrac{\rho_{AFM}^2}{\kappa^2\bar{\epsilon}W}}, \quad S_s(d_0) \approx 2W - \frac{16}{3}W\frac{1}{\ln\kappa d_s}. \quad (43)$$

Equations (42) and (43) are valid to leading order in $\kappa d \ll 1$; even though $\ln\kappa d_s$ is thus large, the relatively large coefficient of 16/3 in the second term of Eq. (43) allows for a significant reduction of domain wall energy due to the presence of a stripe of antiferromagnetic phase. It is not impossible that this reduction can make the quantity S_s lower than the Bloch wall energy S_B, provided that the easy-axis anisotropy constant K is sufficiently large. The domain walls would then have a stripe structure and would strongly interfere with the transport properties of the system. However, the exact values of quantities κ and W in Eq. (43) are not known, and it is not clear whether this situation can be realized experimentally.

More importantly, Eq. (43) [and its 3D analog, Eq. (B15)] refer to the case when phase separation is just beginning, with the islands of antiferromagnetic phase separated by large areas of a ferromagnet. Indeed, our derivation relied on an assumption that the screening clouds formed around different antiferromagnetic islands do not overlap, that is, that the interisland distance is much larger than the screening radius. The size of each island, on the other hand, is much smaller than κ^{-1}, so only a small part of the net sample area is occupied by the antiferromagnetic phase, making phase separation difficult to detect. The available experimental data on phase separation in the CMR compounds,[21] on the other hand, correspond to the case when a substantial part of the sample reverts to a nonferromagnetic phase. Within the context of the phase separation mechanism considered here this is only possible when neither the size of the antiferromagnetic islands (or stripes) nor the interisland distance is larger than Debye-Hückel radius. Below we will consider the case when screening is negligible (that is, when the interisland distance is much smaller than κ^{-1}). Since κ is expected to be small (see above), this is not unrealistic; moreover, the results are expected to provide a reasonable estimate for the case of intermediate screening strength as well.

The ferro- and antiferromagnetic phases are then characterized by uniform values of electron densities x_{FM} and x_{AFM} and charge densities, $\rho_{FM} = -e(x_{FM} - x)$ and $\rho_{AFM} = -e(x_{AFM} - x)$. The numbers of sites occupied by ferro- and antiferromagnetic phases,

$$N_{FM} = \frac{N}{1+\delta}, \quad N_{AFM} = \frac{N\delta}{1+\delta}, \quad \delta \equiv -\frac{\rho_{FM}}{\rho_{AFM}} \quad (44)$$

(where N is the total number of sites in the system), are self-adjusted in such a way that the values of the bulk thermodynamic potentials of the two phases, Ω_{FM} and Ω_{AFM}, are close to each other. Therefore our observation that both the spin stiffness DS and abrupt wall energies are significantly reduced and are of the same order of magnitude (see above and Fig. 6) remains applicable.

It is expected that the value of the parameter δ can be determined experimentally.

We are interested in the situation when within each ferromagnetic domain the poorly conducting antiferromagnetic phase forms disconnected droplets (so that metallic conductance through the connected ferromagnetic area is still possible), and we will again assume that these droplets are circular in shape. The number of droplets in the sample is then $N_{AFM}/(\pi R^2)$ (where R is the radius of a droplet), and thermodynamic potential of the phase-separated system is given by

$$\Omega_1(R) = \frac{\Omega_{FM} + \Omega_{AFM}\delta}{1+\delta} + \frac{1}{\pi R^2}\frac{\delta}{1+\delta}(2\pi RW + E_1) \quad (45)$$

per site, where E_1 is the Coulomb energy of a single droplet. This term cannot be evaluated rigorously; in order to estimate it, we calculate the energy of the Coulomb interaction within the so-called Wigner cell, composed of the droplet and a surrounding ring $R < r < R'$ (where r is the distance from the center of the droplet) of the ferromagnetic phase. The value of $R' = R[(1+\delta)/\delta]^{1/2}$ is chosen in such a way that the combined charge of the droplet and ring vanishes. It should be emphasized that unless δ is small, $\delta \ll 1$, this procedure, which has been used to treat a similar problem earlier,[53] is not exact[54]: even though the electrostatic potential of a Wigner cell falls off rapidly with distance, $\varphi(r) \propto r^{-3}$, it does not vanish outside the cell. In addition, different Wigner cells overlap with each other. Thus, by using this approach we essentially replace the Coulomb force with some model interaction, which, however, captures the essential features of the original problem as long as the value of δ is not too large (see below). We find $E_1 = 8\pi(R')^2R\rho_{AFM}^2A_1(\delta)\delta/(3\bar{\epsilon})$ [see Appendix B, Eq. (B17)], where for small values of $\delta \ll 1$ the function $A_1(\delta)$ is equal to 1. The thermodynamic potential of the droplet phase, Eq. (45), has to be minimized with respect to the droplet radius R, yielding

$$\Omega_1 = \frac{\Omega_{FM} + \Omega_{AFM}\delta}{1+\delta} + \frac{8|\rho_{FM}|}{\sqrt{1+\delta}}\sqrt{\frac{A_1(\delta)W}{3\bar{\epsilon}}}. \quad (46)$$

Another possible geometry of phase separation is represented by the stripe phase [shown in Fig. 8(a)], formed by the parallel antiferromagnetic stripes of width d embedded into the ferromagnetic background. The thermodynamic potential of the stripe phase is given by

$$\Omega_2(d) = \frac{\Omega_{FM} + \Omega_{AFM}\delta}{1+\delta} + \frac{1}{d}\frac{\delta}{1+\delta}(2W + E_2). \quad (47)$$
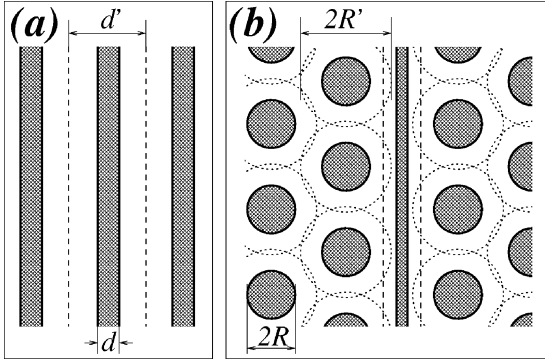
FIG. 8. Stripe phase (a) and stripe domain wall within the droplet phase (b). The system is phase-separated into ferromagnetic (unshaded) and antiferromagnetic (shaded) regions with $\delta \approx 0.4$. The Wigner-cell boundaries of stripe and droplet phases are shown with dashed and dotted lines, respectively. The two connected ferromagnetic domains extending to the left and to the right of the stripe wall in (b) are magnetized in the opposite directions (not shown). The width of antiferromagnetic stripes in (a) and (b) is given by Eqs. (48) and (49), respectively.
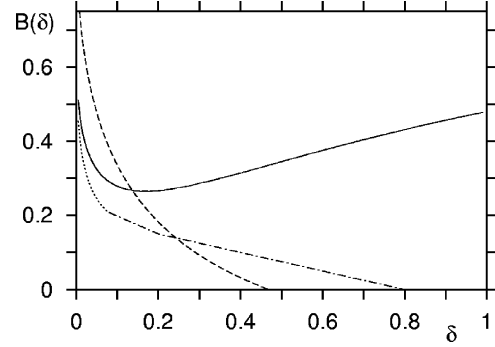

FIG. 9. The ratio B of the energy of a stripe wall to that of an abrupt wall [see Eq. (50)] vs the ratio δ of antiferro- and ferromagnetic areas of the sample: solid line, droplet phase; dotted line, square-droplet phase at low δ; dash-dotted line, possible behavior for the square-droplet phase at larger δ; dashed line, 3D result of Eq. (B23).

Within the Wigner-cell approximation, the Coulomb energy per unit length of a single stripe, E_2, is calculated by subdividing the sample into "Wigner stripes" of width $d' = d(1+\delta)/\delta$ [see Fig. 8(a)]. We find $E_2 = -[dd'\rho_{AFM}^2 A_2(\delta)\delta/\bar{\epsilon}]\ln\delta$ with $A_2(\delta \to 0) = 1$ [see Appendix B, Eq. (B19)]. Minimizing the value of Ω_2 with respect to d, we obtain

$$d_0 = \frac{1}{|\rho_{AFM}|}\sqrt{\frac{2W\bar{\epsilon}}{(1+\delta)A_2(\delta)|\ln\delta|}},$$

$$\Omega_2 - \Omega_1 = \frac{|\rho_{FM}|}{\sqrt{1+\delta}}\sqrt{\frac{W}{\bar{\epsilon}}}\left(2\sqrt{2A_2(\delta)|\ln\delta|} - 8\sqrt{\frac{A_1(\delta)}{3}}\right).$$

(48)

The latter quantity is positive for all values of δ between 0 and 1, indicating that within this model approach, the droplet phase is always preferred (see below). The formation of a stripe domain wall in the droplet phase involves rearranging spins within a Wigner stripe of width $d_s' = d_s(1+\delta)/\delta$ into the stripe phase [see Fig. 8(b)], that is, forming a single stripe of antiferromagnetic phase [of width $d_s(\delta)$] flanked by two stripes of ferromagnet. The net area occupied by the antiferromagnetic phase, N_{AFM}, is conserved, as is the overall electric neutrality. Minimizing the stripe wall energy per unit length, $S_s = (\Omega_2(d_s) - \Omega_1)d_s'$, with respect to d_s, we find

$$d_s = \frac{4}{A_2(\delta)|\rho_{AFM}\ln\delta|}\sqrt{\frac{W\bar{\epsilon}A_1\delta}{3(1+\delta)}},$$

(49)

$$S_s = 2WB(\delta), \quad B(\delta) = 1 - \frac{8}{3}\frac{A_1(\delta)}{A_2(\delta)|\ln\delta|}.$$

(50)

The ratio $B(\delta)$ of the stripe wall energy S_s to the abrupt wall energy, $2W$, is plotted in Fig. 9 (solid line). We see that the

inclusion of an antiferromagnetic stripe can lower the energy of an abrupt wall by a factor of 4. Since the spin stiffness DS is of the same order as the abrupt wall energy (see Fig. 6), the stripe wall energy can be lower than the Bloch wall energy S_B already at a moderate value of anisotropy, $K \sim DS/64$ [cf. Eq. (2)].

Within the Wigner-cell approach for circular droplets the other droplet phase, with the ferromagnetic droplets in the antiferromagnetic background, becomes preferred at $\delta > 1$ (cf. Ref. 53). While this transition might give rise to new possible domain wall structures near $\delta = 1$, this is not expected to be physically relevant due to the intrinsic limitations of the method. As the value of δ increases towards unity, the Wigner-cell estimate for the Coulomb energy becomes progressively less reliable due to decreasing separation between the droplets. It is perhaps even more important that the effects of droplet shape can no longer be ignored.

As mentioned above, it is likely that the optimal shape of antiferromagnetic droplets is square; this would be in line with earlier results for the double-exchange model,[22] as well as with the numerical results for phase separation in other similar systems.[55] In order to calculate the energy of the square-droplet phase at small δ, one can still use the Wigner-cell approach. Due to the increase in the droplet boundary energy, the combined Coulomb and boundary contribution to the thermodynamic potential of the droplet phase [the last term in Eq. (46)] increases by some 6%. This in turn leads to a noticeable decrease in the quantity $B(\delta)$ (dotted line in Fig. 9).

As the value of δ increases, the Wigner-cell method becomes completely unsuitable for the analysis of the square-droplet phase. Indeed, at $\delta = 1$ (that is, at $N_{FM} = N_{AFM}$) the square-droplet phase corresponds to a checkerboard arrangement of equal ferro- and antiferromagnetic squares, which has nothing in common with the Wigner-cell picture (cf. Fig. 8). It is therefore clear that the thermodynamic potential of the square-droplet phase at sufficiently large δ is well above the value given by Eq. (46). Accordingly, Eq. (50) significantly overestimates the value of $B(\delta)$ and hence the stripe wall energy, S_s. While leaving this subject for future inves-

tigation, we note that it is entirely possible that at a certain value of $\delta = \delta_c < 1$ the thermodynamic potential of the square-droplet phase exceeds that of the stripe phase, Eq. (47). The quantities $B(\delta)$ and S_s will vanish at this point,[56] as exemplified schematically by the dash-dotted line in Fig. 9. In this case, for any finite value of the anisotropy constant $K > 0$ and sufficiently small $\delta_c - \delta > 0$, magnetic domain walls within the conducting phase would have stripe (as opposed to Bloch-like) structure.

We close with a brief comment on the applicability of our analysis to finite-thickness films. The results of Secs. II and III for the spin stiffness and abrupt wall energies are valid only as long as the carrier velocity component perpendicular to the film is negligible. However, our conclusion that on the brink of phase separation DS and the abrupt wall energies are generally of the same order of magnitude (as illustrated by Fig. 6) is likely to remain valid in 3D as well. Our assumption that the screening has two-dimensional character is valid as long as the film thickness remains small in comparison with the two-dimensional Debye-Hückel radius κ^{-1}. The film is then thin from the viewpoint of electrostatics [cf. Eq. (B5)]; that is, there is no electric field in the perpendicular direction within the film.[57] The latter holds provided that the film itself is homogeneous in this direction, i.e., that characteristic length scale of a phase-separated sample [the droplet radius, $R \sim (\bar{\epsilon} W)^{1/2} / |\rho_{AFM}|$] is larger than the film thickness. Given the typical experimental observations[21] that phase separation occurs on the scale of at least 50–100 nm, this last condition is not particularly restrictive.

The Debye radius can be roughly estimated by assuming that ν_0 is of the order of the inverse bandwidth ($4t \sim 5$ eV) divided by the unit cell area (~ 0.15 nm^2). Taking, in Eq. (37), $\epsilon_{d2} = 1$ (dielectric constant of the air), we then find $\kappa^{-1} \sim (\epsilon_{d1} + 1) \times 0.08$ nm. The substrate used in the measurements of Ref. 6, lanthanum aluminate, has the dielectric constant[58] of $\epsilon_{d1} \approx 24$, resulting in $\kappa^{-1} \sim 2$ nm. It is therefore tempting to associate the reported domain wall resistance[6] (large for the thinnest $Pr_{2/3}Sr_{1/3}MnO_3$ films of 4 nm, vanishing for films thicker than 20 nm), which is observable below the Curie temperature $T_C \approx 130$ K, with the stripe walls which arise only as long as the thickness of the conducting layer (which is presumably somewhat thinner that the film itself) is not large[59] in comparison with κ^{-1}. We note that the film thickness required for the lattice periods (and hence the anisotropy constant K and Bloch wall energy) to relax to their bulk values is of the order of 500 nm (cf. Ref. 7). Thus, our suggestion provides an (hitherto lacking) interpretation for the disappearance of domain wall resistivity in films thicker than only 20 nm.

The experiments of Ref. 5, on the other hand, were performed with (ferroelectric) strontium titanate substrate, with[60] $\epsilon_{d1} \approx 1200$ at $T = 110$ K, which yields $\kappa^{-1} \sim 100$ nm. The $La_{0.7}Ca_{0.3}MnO_3$ (with Curie temperature $T_C = 250$ K) film[5] was 200 nm thick, and the domain wall contribution was observable below $T = 110$ K. Given the strong dependence of ϵ_{d1} on temperature ($\epsilon_{d1} \approx 24\,000$ at low T, $\epsilon_{d1} \approx 300$ at room temperature), it appears plausible that domain walls have stripe structure at low temperatures, when

the film thickness is not large in comparison with κ^{-1}. Furthermore, it is not unlikely that the above-mentioned transition at $T \approx 110$ K is due to the violation of this condition at larger T and associated change of the domain wall structure.[61] We emphasize that this discussion is speculative at best, as we make no attempt to adequately describe the crossover between two- and three-dimensional screening or to take into account the peculiar geometry of the sample used in Ref. 5.

It appears that stripe wall formation is in principle also possible in the opposite limiting case of a bulk 3D material, although the Wigner-cell estimates given in Appendix B suggest that somewhat higher values of δ are required. The values of the Debye radius $\kappa^{-1}_{(3D)}$ and dielectric constant ϵ_d of doped manganates are, however, not known, and, crucially, very small values of anisotropy make the Bloch wall energy very low. It is therefore expected that in the 3D case the energy of the Bloch wall is generally lower than that of a stripe wall, in agreement with the fact that no observable domain wall contribution to resistivity was reported for the manganate crystals.

V. DISCUSSION

In this article we showed that there are at least three different possible types of structure of a ferromagnetic domain wall, *all of which can be realized within the double-exchange model*. The energies and charges of Bloch, abrupt, and stripe domain walls are also different, as are their anticipated contributions to the resistance and magnetoresistance of the sample. The conventional, weakly charged Bloch walls (Sec. II), which generally arise in single-phase samples, become unstable at low carrier densities, when the abrupt walls (Sec. III) are preferred. For a phase-separated system, however, there is a region of parameter values when the domain walls acquire stripe structure (Sec. IV), characterized by a stripe of antiferromagnetic phase separating the two domains.

It is not yet known whether all three types of wall can occur in the CMR manganate compounds. As follows from the discussion in Sec. III, abrupt walls are expected to arise at low values of electron doping,[62] $x \ll 1$, provided that the homogeneous ferromagnetic phase remains thermodynamically stable. We are not aware of any measurements of the domain wall contribution to transport in this regime, and it is not clear whether such a situation (which also requires the value of direct superexchange J to be extremely small) can be realized in the manganates (however, see the end of Sec. III for a discussion of other compounds). As for the intermediate doping values, it appears that domain walls can have either stripe or Bloch structure.

The effect of Bloch walls on the charge transport properties of a double-exchange ferromagnet has been discussed theoretically.[63] The results are consistent with simpler estimates[5–7] suggesting that for a realistic value of l_B and at an intermediate doping level, carrier scattering off the Bloch wall cannot possibly account for a measured domain wall contribution to the resistivity of the systems studied in Refs. 5–7. Measurable domain wall contributions to the transport properties of the CMR manganates, reported in other studies

known to us, are attributable to the grain boundary effects in polycrystalline films.[9,11,64] In this case, the magnetic structure[10,11] of a domain wall arising at a substrate grain boundary is largely determined by underlying lattice defects.[65] It is anticipated that this also holds for the magnetic pattern appearing in a strained film at the boundary of a heavy-ion-irradiated region.[66] We note that the effects of lattice irregularities of any type are not included in the present theoretical treatment.

Our results suggest that magnetic domain walls in monocrystals or epitaxial films of CMR manganates at the intermediate doping levels generally have Bloch-like structure, with a notable exception of certain strained films similar to those used in Refs. 5–7. Regarding the latter case, we expect that domain walls may in fact be the stripe walls introduced in Sec. IV above. This suggestion is corroborated by the especially strong effect reported in Ref. 6, which shows that domain walls give a dominant contribution to the resistivity of a thin $Pr_{2/3}Sr_{1/3}MnO_3$ film at low temperatures. The connection between domain wall resistivity and dielectric properties of the substrate, discussed in the end of Sec. IV, appears to lend further support to the stripe wall scenario. The stripe walls appear likely to arise in this case due to the strain-induced increase of the easy-axis anisotropy constant K (which in turn increases the Bloch wall energy) and also to phase separation which makes the formation of the stripe walls possible. While it is not clear whether phase separation does occur in the samples used in Refs. 5–7, this would be rather plausible given that phase separation is commonly observed in both manganate crystals and films.[21] We suggest that further measurements (e.g., scanning tunneling spectroscopy) need to be carried out to clarify whether these samples are in fact phase separated. On the other hand, domain wall properties (including possible domain wall contributions to the resistivity) of those CMR films which *are* known to phase separate[21,67] should also be investigated. Synthesis of electron-doped manganate films, if technologically possible, may represent a promising new direction.[38] We note that magnetic domain walls appear only when a substantial fraction of the film is in the ferromagnetic state, allowing for a low-field metallic conduction.

In the present article, we did not quantitatively address the problem of conduction across a domain wall of either type. The available theoretical estimates of domain wall conductance (Ref. 63 for Bloch walls, Ref. 16 for abrupt walls) are incomplete in that the Coulomb interaction between the carrier and (charged) domain wall is not taken into account. As for the stripe walls, the issue of magnetotransport in this case has yet to be treated theoretically, although it is clear that the stripe wall contribution to resistivity is much larger than that of either Bloch or abrupt walls. In the presence of stripe domain walls, magnetoresistance will be affected by the change of their structure under a magnetic field, which is likely to include a field-driven transition from stripe to Bloch walls. It is therefore expected that the dependence of the domain wall contribution to resistivity on the magnitude of the applied in-plane field can be different for the Bloch and stripe cases (a smooth decrease for Bloch walls, as opposed

to possibly steplike features for stripe walls, as seen in Ref. 5).

Magnetotransport studies are not the only way to investigate the properties of magnetic domain walls. Direct probes of the charge and spin structure of domain walls are possible in principle (cf. Ref. 68), but have not yet been performed for the manganates. However, Fresnel imaging measurements on a thin $La_{0.7}Ca_{0.3}MnO_3$ film were reported recently.[8] Domain walls were found to retain a finite width of the order of 40 nm, in apparent agreement with Eq. (2) for Bloch walls. We hope that domain wall widths in the strained films studied in Refs. 5–7 will also be measured in the near future. It would be most interesting to try to relate these to the band structure, magnetic, and electrostatic properties of the corresponding compounds and to check the agreement with the estimates (43) and (49) for the stripe walls.

APPENDIX A: DERIVATION AND ANALYSIS OF EQS. (33)–(34)

The key step in the calculation of the spectral shift function, Eq. (32), is the diagonalization of perturbation operator V_{k_x} [see Eqs. (24) and (25)]. Its eigenvalues A_i and the corresponding fermionic operators a_i are given by

$$A_1 = A_2 = -A_3 = -A_4 = -\frac{Q}{2\sqrt{2}}\psi^2, \qquad (A1)$$

$$A_5 = A_6 = -A_7 = -A_8 = -\frac{Q}{\sqrt{2}}(1-\psi), \qquad (A2)$$

and

$$8(2\pm\sqrt{2})^{1/2}a_{1,3} = (4-\psi^2)(d_{-1\uparrow}+d_{2\uparrow})+[(4\pm2\sqrt{2})\psi$$
$$+(4\pm\sqrt{2})\psi^2](d_{0\uparrow}+d_{1\uparrow})$$
$$+(1\pm\sqrt{2})(4-\psi^2)(d_{-1\downarrow}-d_{2\downarrow})$$
$$+[\mp2\sqrt{2}\psi-(2\pm3\sqrt{2})\psi^2](d_{0\downarrow}-d_{1\downarrow}),$$
$$(A3)$$

$$8(2\mp\sqrt{2})^{1/2}a_{2,4} = -(4-\psi^2)(d_{-1\uparrow}-d_{2\uparrow})+[(4\mp2\sqrt{2})\psi$$
$$+(4\mp\sqrt{2})\psi^2](d_{0\uparrow}-d_{1\uparrow})$$
$$+(-1\pm\sqrt{2})(4-\psi^2)(d_{-1\downarrow}+d_{2\downarrow})$$
$$+[\pm2\sqrt{2}\psi-(2\mp3\sqrt{2})\psi^2](d_{0\downarrow}+d_{1\downarrow}),$$
$$(A4)$$

$$8(2\mp\sqrt{2})^{1/2}a_{5,7}=-2\sqrt{2}(\psi+\psi^2)(d_{-1\uparrow}+d_{2\uparrow})+(\sqrt{2}\mp1)$$

$$\times\left[4\pm2(\sqrt{2}\pm1)\psi-\frac{3}{2}\psi^2\right](d_{0\uparrow}+d_{1\uparrow})$$

$$\pm(4\mp2\sqrt{2})(\psi+\psi^2)(d_{-1\downarrow}-d_{2\downarrow})$$

$$+\left[\pm4-2(\sqrt{2}\mp1)\psi\mp\frac{3}{2}\psi^2\right](d_{0\downarrow}-d_{1\downarrow}),$$

$$(A5)$$

$$8(2\pm\sqrt{2})^{1/2}a_{6,8}=2\sqrt{2}(\psi+\psi^2)(d_{-1\uparrow}-d_{2\uparrow})+(\sqrt{2}\pm1)$$

$$\times\left[4\mp2(\sqrt{2}\mp1)\psi-\frac{3}{2}\psi^2\right](d_{0\uparrow}-d_{1\uparrow})$$

$$\pm(4\pm2\sqrt{2})(\psi+\psi^2)(d_{-1\downarrow}+d_{2\downarrow})$$

$$+\left[\mp4-2(\sqrt{2}\pm1)\psi\pm\frac{3}{2}\psi^2\right](d_{0\downarrow}+d_{1\downarrow}).$$

$$(A6)$$

These expressions are then used to form the matrix elements M_{ij} (see Eq. (29)), for example

$$M_{11}=\frac{2-\sqrt{2}}{4Q}(4E_\uparrow^2-1)-\frac{2+\sqrt{2}}{4Q}(4E_\downarrow^2-1)$$

$$+(2-\sqrt{2})(1+3E_\uparrow-4E_\uparrow^3)I_\uparrow$$

$$+(2+\sqrt{2})(1-3E_\downarrow+4E_\uparrow^3)I_\downarrow+\mathcal{O}(\psi),$$

$$I_\alpha=\frac{1}{8\pi Q}\int\frac{dk_y}{E_\alpha+\cos k_y-i0}\qquad(A7)$$

[see Eq. (30)]. Note that, owing to the symmetry properties of the operators a_i, the quantities M_{ij} vanish unless both indexes i and j are either odd or even. Hence the 8×8 determinant on the RHS of Eq. (28) reduces to a product of two 4×4 determinants. After some algebra, one obtains expression (32), which has to be substituted into Eqs. (33) and (35).

In the case of a vertical wall we choose the coordinate axes r_1 and r_2 along the lattice directions with the r_2 axis perpendicular to the wall. After the Fourier transformation

$$d_\alpha(r_1,r_2)=N^{-1/4}\sum_{k_1}e^{ik_1r_1}d_\alpha(k_1,r_2),\qquad(A8)$$

we find that the unperturbed Hamiltonian has the form

$$\tilde{\mathcal{H}}=\sum_{k_1}\left(\mathcal{H}_{k_1}-\cos k_1\sum_{r_2}d_\alpha^\dagger(k_1,r_2)d_\alpha(k_1,r_2)\right),\quad(A9)$$

and the domain wall again results in a local perturbation $\mathcal{H}_{k_1}\to\mathcal{H}_{k_1}+V_{k_1}$. This perturbation is still illustrated by Fig. 3, although the intersite distance is now equal to unity, rather than to $1/\sqrt{2}$. The operators $\mathcal{H}_{k_1}$ and V_{k_1} have the same form as $\mathcal{H}_{k_x}$ and V_{k_x} [see Eqs. (23) and (24)], with the substitu-

tions $Q\to1$, $d_\alpha(k_x,y+1/\sqrt{2})\to d_\alpha(k_1,y+1)$, $d_\alpha(k_x,i/\sqrt{2})\to d_\alpha(k_1,i)$. Hence Eqs. (A1)–(A6) with the value of Q set to unity can be used to diagonalize the perturbation [see Eq. (25)] in the case of a vertical wall as well.

We note that in the expressions for both $\mathcal{H}_{k_1}$ and V_{k_1} in terms of the operators $d_\alpha(k_1,r_2)$, the coefficients do not depend on k_1. Therefore, the only effect of the second term on the RHS of Eq. (A9), regardless of whether the domain wall is present, is to shift all of the energy levels by $-\cos k_1$. Thus, Eqs. (26) and (27) are now replaced by

$$\Omega=\int\frac{L_1dk_1}{2\pi}\int d\epsilon_2\,\nu_{tot2}(\epsilon_2)\varphi(\epsilon_2+\epsilon_1),$$

$$\frac{\delta\Omega}{L_1}=\int\frac{dk_1}{2\pi}\int d\epsilon_2\,\delta\nu_2(\epsilon_2)\varphi(\epsilon_2+\epsilon_1)$$

$$=\int\frac{dk_1}{2\pi}\int d\epsilon_2\,\tilde{\xi}(\epsilon_2)f(\epsilon_2+\epsilon_1),$$

$$\epsilon_{1,2}=-\cos k_{1,2},\qquad\nu_{tot2}(\epsilon_2)=L_2/(\pi\sqrt{1-\epsilon_2^2}).$$

$$(A10)$$

Here, L_1 and L_2 are the dimensions of the sample, and $\tilde{\xi}(\epsilon)$ is the spectral shift function of the corresponding 1D problem. It is evaluated as $\pi\tilde{\xi}(\epsilon)=-\mathrm{ArgDet}(\delta_{ij}-\tilde{M}_{ij}A_j)$, with

$$\tilde{M}_{ij}=\sum_{\alpha=\uparrow,\downarrow}\int\frac{dk_2}{2\pi}\frac{\langle0|a_i|k_2^\alpha\rangle\langle k_2^\alpha|a_j^\dagger|0\rangle}{E_\alpha+\cos k_2-i0}\qquad(A11)$$

and $E_\uparrow=E_\downarrow+J_H=\epsilon$. Taking also into account that the states $|k_2^\alpha\rangle$ are defined in a conventional way, $|k_2^\alpha\rangle=\sum_{r_2}\exp(-ik_2r_2)d_\alpha^\dagger(k_1,r_2)|0\rangle$ [cf. Eq. (31)], we conclude that the value of $\tilde{M}_{ij}$ coincides with that of M_{ij}, Eq. (29), calculated at $Q=1$. Thus, $\tilde{\xi}(\epsilon)=\xi(\epsilon,Q=1)$ [see Eq. (32)], and Eqs. (34) and (36) follow.

The somewhat cumbersome expressions (32)–(36) become much simpler in the case of a large Hund's rule coupling $J_H\to\infty$. We then find[69]

$$S_d=\frac{1}{\sqrt{2}}\left\{\frac{\sqrt{4-\mu^2}}{\pi}-\frac{|\mu|}{\pi}\arccos\frac{|\mu|}{2}-4J+E-\mu[x-\theta(\mu)]\right\}$$

$$+2\sqrt{2}\left\{2J+K+\frac{4}{3\pi^2}\left[\frac{\mu^2}{2}Y_1-\left(1+\frac{\mu^2}{4}\right)Y_2\right]\right\}\psi^2,$$
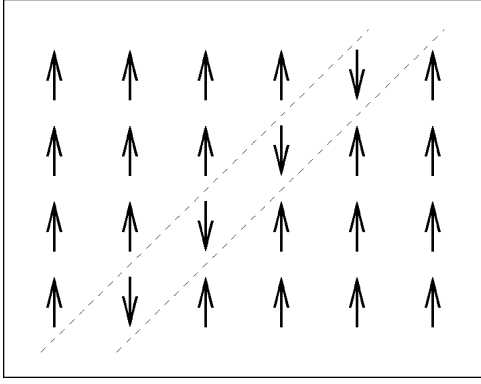
$$(A12)$$

FIG. 10. Local perturbation used in the calculation of abrupt domain wall energies at $J_H \to \infty$ (for the case of a diagonal wall).

$$S_v = \frac{\sqrt{2|\mu| - \mu^2}}{2\pi} + \frac{1 - |\mu|}{2\pi} \arccos(|\mu| - 1) - 2J + E$$

$$- \mu[x - \theta(\mu)] + 4\left\{ J + K - \frac{4}{9\pi^2}\left[\left(\mu^2 + \frac{3}{8}\mu^4\right)Y_1 \right.\right.$$

$$\left.\left. + \left(1 - \frac{11}{4}\mu^2\right)Y_2\right]\right\}\psi^2, \qquad (A13)$$

$$\sigma_d = -\frac{e}{\pi\sqrt{2}}\arccos\frac{|\mu|}{2}\operatorname{sgn}\mu - \frac{e}{\sqrt{2}}[x - \theta(\mu)],$$
$$(A14)$$

$$\sigma_v = -\frac{e}{2\pi}\arccos(|\mu| - 1)\operatorname{sgn}\mu - e[x - \theta(\mu)],$$
$$(A15)$$

where Y_i and E are given by Eqs. (5) and (6). When deriving the $\psi = 0$ values of S_d and S_v above, it is convenient to use a calculation scheme somewhat different from that used in the finite-J_H case. Namely, the local perturbation we consider now (see Fig. 10) corresponds to inverting the spins along a 1D chain, not only shutting the carrier hopping, but also introducing a single chain of an antiferromagnetic phase. The latter circumstance can easily be accounted for by subtracting the difference of thermodynamic potentials between the antiferro- and ferromagnetic phases; the advantage of this method lies in a very simple form of the spectral shift function, $\xi(\epsilon, Q) = (1/2)\operatorname{sgn}\epsilon$, corresponding to the perturbation shown in Fig. 10.

Another potentially important case when the integration in Eqs. (33)–(36) can be carried out analytically is that of small electron densities $x \ll 1$. For any value of $J_H \gg x$, we obtain

$$S_d \approx \frac{4\sqrt{\pi}}{3}x^{3/2} - \pi\sqrt{\frac{J_H + 4}{2J_H}}x^2 - 2\sqrt{2}J$$

$$+ \sqrt{2}\left\{\pi J_H\left(1 - \sqrt{1 + \frac{4}{J_H}}\right)x^2 + 4J + 2K\right\}\psi^2,$$

$$(A16)$$

$$S_v \approx \frac{4\sqrt{\pi}}{3}x^{3/2} - \pi\sqrt{\frac{J_H + 2}{J_H}}x^2 - 2J$$

$$+ 4\left\{\pi J_H\left(1 - \sqrt{1 + \frac{2}{J_H}}\right)x^2 + J + K\right\}\psi^2. \quad (A17)$$

It is instructive to note that expansion of these expressions in the case of $J_H \gg 1$ shows that the leading $1/J_H$ correction amounts to a renormalization of the superexchange constant, $J \to J + (\pi x^2)/(2J_H)$. This is another illustration of an effective antiferromagnetism being induced by a finite Hund's rule coupling, as discussed in Sec. II. We also see that at $J = 0$ and to leading order in $x \ll 1$, abrupt wall energy does not depend on the orientation of the wall, $S_d^{(0)} = S_v^{(0)}$, which is due to the carrier dispersion law being isotropic at low densities.

The electric charges of unperturbed abrupt domain walls at $x \ll 1, J_H$ are given by

$$\sigma_d \approx e\sqrt{\frac{x}{\pi}} - ex\sqrt{\frac{J_H + 4}{2J_H}} - ex^{3/2}\frac{\sqrt{\pi}}{24}, \qquad (A18)$$

$$\sigma_v \approx e\sqrt{\frac{x}{\pi}} - ex\sqrt{\frac{J_H + 2}{J_H}} + ex^{3/2}\frac{\sqrt{\pi}}{24}. \qquad (A19)$$

Finally, we also quote a 3D result for a vertical abrupt domain wall energy (per unit area) at $x \ll 1$ and $J_H \to \infty$:

$$S_v^{(3D)} \approx \frac{2^{1/3}3^{4/3}}{16}\pi^{5/3}x^{4/3} - 2J, \quad \psi = 0. \qquad (A20)$$

APPENDIX B: STRIPE WALLS AND SCREENING

In this appendix, we are concerned predominantly with the investigation of the screening potentials and Coulomb energies of phase-separated states in a two-dimensional conductor. Let the values of the dielectric constants of the media on both sides of conducting plane be ϵ_{d1} and ϵ_{d2}. The method of images enables one to evaluate the potential of a point charge q located at a distance z from a plane separating the two dielectric media.[14] In the limit $z \to 0$, we find that this potential at any point in space is given by $q/(\bar{\epsilon}s)$, where s is the distance from the charge and $\bar{\epsilon} = (\epsilon_{d1} + \epsilon_{d2})/2$. We therefore conclude that the electrostatic properties of this system are described by a Poisson's equation of the form

$$\bar{\epsilon}\nabla^2\varphi = -4\pi\rho(\vec{r})\delta(z). \qquad (B1)$$

Here, $\vec{r} = \{x, y\}$ is the 2D radius vector in the plane, the z axis is perpendicular to the conductor, and ∇ is the usual 3D gradient. It is therefore only the effective dielectric constant $\bar{\epsilon}$ that will affect the values of physical quantities in this case [cf. Eq. (37)].

We begin with evaluating the potential of a charged string within the film. Assuming that the string coincides with the x axis, we rewrite Eq. (B1) as

$$\bar{\epsilon}\nabla^2\varphi(y,z) = [4\pi e^2\varphi(y,z)\nu_0 - 4\pi\sigma\delta(y)]\delta(z). \quad (B2)$$

Here, σ is the linear charge density of the string, and the first term on the RHS accounts for a screening charge arising from the band energy shift by the electrostatic energy, $-e\varphi$. This is a standard Thomas-Fermi treatment of screening, valid in the long-wavelength limit. Upon one-dimensional Fourier transformation we obtain

$$\left(\frac{\partial^2}{\partial z^2} - k_y^2\right)\varphi(k_y, z) = \left(2\kappa\varphi(k_y, z) - \frac{4\pi\sigma}{\bar{\epsilon}}\right)\delta(z).$$

(B3)

Using the Green's function for Eq. (B3) (cf. Ref. 46),

$$g(k_y, z) = \int_{-\infty}^{\infty} \frac{dk_z}{2\pi} \frac{e^{ik_z z}}{k_z^2 + k_y^2} = \frac{1}{2|k_y|}e^{-|k_y z|},$$

(B4)

we obtain

$$\varphi(k_y, z) = \frac{1}{|k_y|}e^{-|k_y z|}\left(\frac{2\pi\sigma}{\bar{\epsilon}} - \kappa\varphi(k_y, 0)\right).$$

(B5)

Hence, at $z = 0$, $\varphi(k_y) = 2\pi\sigma/[\bar{\epsilon}(|k_y| + \kappa)]$, and

$$\varphi(y) = \frac{-2\sigma}{\bar{\epsilon}}(\cos\kappa y\,\mathrm{ci}\kappa y + \sin\kappa y\,\mathrm{si}\kappa y),$$

(B6)

where si and ci are sine and cosine integrals. At $\kappa y \gg 1$, Eq. (B6) yields $\varphi(y) \approx 2\sigma/(\bar{\epsilon}\kappa^2 y^2)$. Along with the $1/r^3$ decay of a screened point charge potential,[45,46] this is in contrast with the well-known exponential behaviors found in 3D.

Let us now consider the potential of an antiferromagnetic stripe of width $d \ll \kappa^{-1}$, centered around the x axis. At $y \gg d$, it is given by Eq. (B6) with $\sigma = \rho_{AFM}d$, whereas at $y \ll \kappa^{-1}$ it should coincide with the unscreened potential of the stripe,

$$\varphi(y) = -\frac{2\rho_{AFM}}{\bar{\epsilon}}\left[\left(\frac{d}{2} - y\right)\ln\left|\frac{d}{2} - y\right| + \left(\frac{d}{2} + y\right)\ln\left|\frac{d}{2} + y\right| - d\right]$$

$$+ \mathrm{const.}$$

(B7)

At $y \gg d$, the latter expression takes the familiar form

$$\varphi(y) = -\frac{2\sigma}{\bar{\epsilon}}\ln|y| + \mathrm{const.}$$

(B8)

The two regions $y \gg d$ and $y \ll \kappa^{-1}$ overlap, enabling us to find the value of const in Eqs. (B7) and (B8), $-2\rho_{AFM}d(C + \ln\kappa)/\bar{\epsilon}$, where $C \approx 0.577$ is Euler's constant. Substituting Eq. (B7) into Eq. (39), we find the leading-order expression for the Coulomb energy of the stripe [the last term in Eq. (42)]. It is also easy to estimate the Coulomb energy of a Bloch wall,

$$-\frac{1}{\bar{\epsilon}}\int\int_{-\infty}^{\infty}\delta x(y)\ln|\kappa(y - y')|\delta x(y')dydy' \sim \frac{1}{\bar{\epsilon}}\sigma_B^2\ln|\kappa l_B|$$

(B9)

[see Eq. (18)], assuming that $\kappa l_B \ll 1$.

We note that screening affects the value of the potential at $2|y| < d$ even in the limit of $d \ll \kappa^{-1}$ because the unscreened potential, Eq. (B8), diverges at $y \to \infty$. This is also the case for the potential of a single antiferromagnetic layer of thickness d in a phase-separated sample in three dimensions, in which case we find, per unit area,

$$\frac{1}{2}\int_{AFM}\rho\varphi d^3r \approx \frac{\pi d^2\rho_{AFM}^2}{\kappa_{(3D)}\epsilon_d}, \quad \kappa_{(3D)}^2 = \frac{4\pi e^2\nu_0}{\epsilon_d}.$$

(B10)

In the case of a single antiferromagnetic disk in 2D or an antiferromagnetic sphere (ball) in 3D, the unscreened potential vanishes at large distances and the leading-order (in κR) term in the Coulomb energy does not depend on the screening radius. Indeed, for the 2D case at sufficiently small distances $r \ll \kappa^{-1}$, the exact screened potential of a point charge $\pi R^2\rho_{AFM}$ (found in Refs. 45 and 46) is to leading order given by $\pi R^2\rho_{AFM}/(\bar{\epsilon}r)$. For $r \gg R$, this clearly matches the unscreened potential of a charged disk. Therefore screening does not affect the value of φ within the disk, which enters Eq. (39). Using a Green's function procedure similar to Eqs. (B3) and (B4) above, we obtain, for an unscreened disk of radius R,

$$\varphi(r) = \int\varphi(k)e^{i\vec{k}\cdot\vec{r}}\frac{d^2k}{4\pi^2}, \quad \varphi(k) = \frac{4\pi^2\rho_{AFM}R}{\bar{\epsilon}k^2}J_1(kR)$$

(B11)

(where r is the distance from the island center and J_1 is Bessel function), and

$$\frac{1}{2}\int\frac{d^2k}{4\pi^2}\rho(k)\varphi(k) = \frac{2\pi^2\rho_{AFM}R^2}{\bar{\epsilon}}\int_0^{\infty}[J_1(kr)]^2\frac{dk}{k^2},$$

(B12)

leading to Eq. (40), whereas for a 3D sphere of radius R we readily find

$$\frac{1}{2}\int_{AFM}\rho\varphi d^3r \approx \frac{16\pi^2\rho_{AFM}^2R^5}{15\epsilon_d}.$$

(B13)

Equation (41), derived in Sec. III, holds for a thin film. With the help of Eqs. (B10) and (B13), it is easy to obtain a similar phase-separation threshold condition for the 3D (bulk crystal) case,

$$\Omega_{FM} - \Omega_{AFM} > \Delta_0^{(3D)} = \left(\frac{3^5\pi W_{(3D)}^2\rho_{AFM}^2}{5\epsilon_d}\right)^{1/3}.$$

(B14)

Here, $W_{(3D)}$ is the energy per unit area of a ferromagnetic-antiferromagnetic boundary in three dimensions, which can be approximated by half the value of the 3D abrupt wall energy [cf. Eq. (A20)]. The energy of the stripe (layer) domain wall at the phase-separation threshold in 3D is then given by [cf. Eq. (43)]

$$S_s^{(3D)} = 2W_{(3D)}\left(1 - \frac{27}{20}\kappa_{(3D)}R_0^{(3D)}\right),$$

(B15)

per unit area, where

$$R_0^{(3D)} = \left(\frac{15 \epsilon_d W_{(3D)}}{8 \pi \rho_{AFM}^2} \right)^{1/3}$$

is the radius of antiferromagnetic bubbles appearing immediately above the threshold, Eq. (B14).

We now turn to the other regime of phase separation considered in Sec. IV. In this case, screening is negligible and our estimates of Coulomb contributions to the thermodynamic potential are based on evaluating the electrostatic energy of a single unscreened Wigner cell. In the case of circular antiferromagnetic islands ("droplet phase"), the Fourier component of the electric potential of a Wigner cell is given by [cf. Eq. (B11)]

$$\varphi(k) = \frac{4 \pi^2 R'}{\bar{\epsilon} k^2 R} \rho_{FM} [R J_1(kR') - R' J_1(kR)]. \quad \text{(B16)}$$

Momentum integration [cf. Eq. (B12)] then yields the expression for the Wigner-cell energy E_1, given in the text above Eq. (46), with

$$\frac{A_1(\delta)}{1+\delta} = 1 + \sqrt{\frac{\delta}{1+\delta}} \left[1 - \frac{3\pi}{4} \, {}_2F_1\left(\frac{1}{2}, -\frac{1}{2}; 2; \frac{\delta}{1+\delta} \right) \right], \quad \text{(B17)}$$

where ${}_2F_1$ is the hypergeometric function.

For the stripe phase, we find the electric potential $\varphi(y)$ of a single "Wigner stripe,"

$$\frac{\bar{\epsilon} \varphi(y)}{\rho_{AFM}} = 2y \delta \ln \left| \frac{d'+2y}{d'-2y} \right| - 2y(1+\delta) \ln \left| \frac{d+2y}{d-2y} \right|$$
$$+ d' \delta \ln \left| \frac{(d')^2 - 4y^2}{d^2 - 4y^2} \right|, \quad \text{(B18)}$$

where y is the distance from the stripe center. We note that at $y \gg d'$, the potential $\varphi(y)$ decays as $1/y^2$. Evaluating the electrostatic energy per unit length, $E_2 = \int_{-d'/2}^{d'/2} \varphi(y) \rho(y) dy / 2$, we obtain the expression given in the text following Eq. (47), where

$$A_2(\delta) \ln \delta = (1+\delta) \ln \frac{4\delta(1+\delta)}{1+2\delta} - \frac{1+2\delta+2\delta^2}{2\delta} \ln(1+2\delta). \quad \text{(B19)}$$

It is also possible to evaluate the Coulomb energy of the stripe phase exactly, taking into account the interaction between different "Wigner stripes." Numerical calculation shows that this leads to an increase of the quantity A_2 by about 8% at $\delta \to 1$ and by only 3% at $\delta = 0.17$ [the latter corresponds to the minimum of $B(\delta)$ in Fig. 9], attesting to the relatively high accuracy of the Wigner-cell method for the stripe phase even in 2D.

Coulomb energies of droplet and layered phase-separated states in 3D were evaluated in Ref. 53. The sum of boundary and Coulomb contributions to the thermodynamic potential equals

$$\tilde{\Omega}_1^{(3D)}(R) = \frac{3\delta}{1+\delta} \frac{W_{(3D)}}{R} + \frac{4\pi}{5\epsilon_d} R^2 \rho_{AFM}^2 A_1^{(3D)}(\delta) \delta, \quad \text{(B20)}$$

$$A_1^{(3D)} = 1 + \frac{3}{2}\delta - \frac{3}{2}\delta^{1/3}(1+\delta)^{2/3}, \quad \text{(B21)}$$

for the droplet phase, and

$$\tilde{\Omega}_2^{(3D)}(d) = \frac{2\delta}{1+\delta} \frac{W_{(3D)}}{d} + \frac{\pi}{6\epsilon_d} d^2 \rho_{AFM}^2, \quad \text{(B22)}$$

for the layered phase. Minimizing expression (B20) with respect to the radius R of spherical antiferromagnetic droplets and then the 3D stripe wall energy per unit area, $S_s^{(3D)} = (\tilde{\Omega}_2^{(3D)}(d_s) - \tilde{\Omega}_1^{(3D)}) d_s'$ [where $d_s' = d_s(1+\delta)/\delta$], with respect to the antiferromagnetic layer thickness d_s, we find

$$d_s^{(3D)} = \frac{3^{5/6} \cdot \sqrt{2\delta}(A_1^{(3D)})^{1/6}}{5^{1/6} \pi^{1/3} |\rho_{AFM}|^{2/3}} \left(\frac{W_{(3D)} \epsilon_d}{1+\delta} \right)^{1/3},$$

$$S_s^{(3D)} = 2 W_{(3D)} B_{(3D)}(\delta), \quad B_{(3D)}(\delta) = 1 - 3\sqrt{\frac{6}{5} A_1^{(3D)} \delta}. \quad \text{(B23)}$$

The ratio $B_{(3D)}(\delta)$ of the energies of stripe and abrupt walls in 3D is plotted in Fig. 9 (dashed line). We see that the stripe wall energy vanishes already within the Wigner-cell method as the value of δ approaches $\delta_c^{(3D)} \approx 0.47$.

---

*Electronic address: golosov@thphys.ox.ac.uk

[1] Q. Lu, C.-C. Chen, and A. de Lozanne, Science **276**, 2006 (1997).

[2] T. Fukumura, H. Suguwara, T. Hasegawa, K. Tanaka, H. Sakaki, T. Kimura, and Y. Tokura, Science **284**, 1969 (1999).

[3] C. Kwon, M.C. Robson, K.-C. Kim, J.Y. Gu, S.E. Lofland, S.M. Bhagat, Z. Trajanovic, M. Rajeswari, T. Venkatesan, A.R. Kratz, R.D. Gomez, and R. Ramesh, J. Magn. Magn. Mater. **172**, 229 (1997).

[4] U. Welp, A. Berger, V.K. Vlasko-Vlasov, Qing'An Li, K.E. Gray, and J.F. Mitchell, Phys. Rev. B **62**, 8615 (2000).

[5] N.D. Mathur, P.B. Littlewood, N.K. Todd, S.P. Isaac, B.-S. Teo, D.-J. Kang, E.J. Tarte, Z.H. Barber, J.E. Evetts, and G. Blamire, J. Appl. Phys. **86**, 6287 (1999).

[6] Qi Li, Y.F. Hu, and H.S. Wang, J. Appl. Phys. **89**, 6952 (2001); Qi Li and H.S. Wang, J. Supercond. **14**, 231 (2001); H. S. Wang and Qi Li (unpublished) (the latter was received upon completion of the present work).

[7] Y. Wu, Y. Suzuki, U. Rüdiger, J. Yu, A.D. Kent, T.K. Nath, and C.B. Eom, Appl. Phys. Lett. **75**, 2295 (1999).

[8] S.J. Lloyd, N.D. Mathur, J.C. Loudon, and P.A. Midgley, Phys. Rev. B **64**, 172407 (2001).

[9] A. Gupta, G.Q. Gong, G. Xiao, P.R. Duncombe, P. Lecoeur, P. Trouilloud, Y.Y. Wang, V.P. Dravid, and J.Z. Sun, Phys. Rev. B

54, 15 629 (1996); D.K. Petrov, A. Gupta, J.R. Kirtley, L. Krusin-Elbaum, and H.S. Gill, J. Appl. Phys. **83**, 7061 (1998).

[10] Y.-A. Soh, G. Aeppli, N.D. Mathur, and M.G. Blamire, J. Appl. Phys. **87**, 6743 (2000); Phys. Rev. B **63**, 020402 (2001).

[11] D.J. Miller, Y.K. Lin, V. Vlasko-Vlasov, and U. Welp, J. Appl. Phys. **87**, 6758 (2000).

[12] Cf. Ref. 5 and N.D. Mathur and P.B. Littlewood, Solid State Commun. **119**, 271 (2001).

[13] k_1 and k_2, directed along the principal directions of the inverse lattice, are not to be mixed with diagonally directed and rescaled k_x and k_y, introduced later in the article.

[14] L.D. Landau and E.M. Lifshits, *Electrodynamics of Continuous Media*, Theoretical Physics, Vol. 8 (Pergamon, New York, 1984).

[15] D.I. Golosov, Phys. Rev. Lett. **84**, 3974 (2000).

[16] S. Zhang and Z. Yang, J. Appl. Phys. **79**, 7398 (1996).

[17] We neglect the magnetostatic energy associated with the domain wall in a film. In this limit the wall has the same structure as in the 3D case considered in Ref. 14, and is more properly called the Landau-Lifshits wall [see, e.g., A. Aharoni, *Introduction to the Theory of Ferromagnetism* (Oxford University Press, Oxford, 2000)]. Our treatment remains valid when the anisotropy axis is parallel to the film, although the spin rotation then takes place in a different plane in spin space (Néel wall).

[18] E.L. Nagaev, Fiz. Tverd. Tela **11**, 2779 (1969) [Sov. Phys. Solid State **11**, 2249 (1970)].

[19] We stress that the magnetic properties of these two systems are by no means identical, which can be seen from Eq. (3), yielding a Heisenberg (cosine) dispersion law at $J_H \to \infty$, but not for any finite J_H value.

[20] E.L. Nagaev, *Colossal Magnetoresistance and Phase Separation in Magnetic Semiconductors* (Imperial College Press, London, 2002), and references therein.

[21] E. Dagotto, T. Hotta, and A. Moreo, Phys. Rep. **344**, 1 (2001), and references therein.

[22] D.I. Golosov, J. Appl. Phys. **91**, 7508 (2002); D.I. Golosov (unpublished).

[23] D.I. Golosov, J. Appl. Phys. **87**, 5804 (2000).

[24] P.W. Anderson and H. Hasegawa, Phys. Rev. **100**, 675 (1955).

[25] The integration variable ϵ_x corresponds to $\cos(k_x/2)$. We also assume that μ is negative; the $\mu > 0$ case is treated similarly.

[26] Bloch wall energy, i.e., the change in the thermodynamic potential associated with the Bloch wall, can also be evaluated in a similar way, thus confirming the classical result (2).

[27] When the principal contribution to the spin stiffness D originates from a large *ferromagnetic* superexchange, $-J \gtrsim x$, the Bloch wall remains stable even when the inequality (20) is violated. Due to the absence of carriers near the center of the wall, the domain wall then becomes impenetrable for electrical current.

[28] In the limit of low hole doping, $1 - x \ll 1$, one similarly finds $16\pi(1-x)DS < K$.

[29] By using the Hamiltonian (1), which does not include Coulomb interactions.

[30] This holds for both finite and infinite values of Hund's rule coupling. In the case of $J_H = \infty$, the carrier wave functions must vanish at the wall, whereas at finite values of J_H, the exponential tail of the spin-up wave function extends into the spin-down magnetic domain and vice versa [see Eq. (10)].

[31] In three dimensions, one finds that the energy per unit area of partition is $\sim x^{4/3}$ [see Eq. (A20)].

[32] It is because of the 1D character of the perturbation that one is able to introduce a spectral shift function in this way; Eq. (27) generalizes the standard Lifshits-Krein trace formula (Ref. 33).

[33] I.M. Lifshits, Usp. Mat. Nauk **7(1)**, 171 (1952); I.M. Lifshits, S.A. Gredeskul, and L.A. Pastur, *Introduction to the Theory of Disordered Systems* (Wiley, New York, 1988), Chap. 5; M.G. Krein, *Topics in Differential Equations and Operator Theory* (Birkhäuser, Basel, 1983), pp. 107–172.

[34] D.I. Golosov, M.R. Norman, and K. Levin, Phys. Rev. B **58**, 8617 (1998).

[35] At these values of J, the uniform ferromagnetic state is typically unstable with respect to phase separation.

[36] We emphasize that this statement applies to the intermediate doping range $x, 1 - x \sim 1$.

[37] Adding a nonzero superexchange, $J > 0$, would (i) result in the diagonal (rather than vertical) abrupt wall being preferred at low x and (ii) give rise to a phase-separation instability within a certain low-x region.

[38] Phase separation was indeed detected in $Ca_{1-x}Sm_xMnO_3$ with $x \approx 0.15$ [see M. Respaud, J.M. Broto, H. Rakoto, J. Vanacken, P. Wagner, C. Martin, A. Maignan, and B. Raveau, Phys. Rev. B **63**, 144426 (2001)]. It is likely that it also occurs in electron-doped monolayered compounds, like $Ca_{2-x}Pr_xMnO_4$ [A. Maignan, C. Martin, G. van Tendeloo, M. Hervieu, and B. Raveau, J. Mater. Chem. **8**, 2411 (1998)].

[39] E.L. Nagaev, Phys. Rep. **346**, 387 (2001), and references therein.

[40] Y. Shapira, S. Foner, N.F. Oliveira, Jr., and T.B. Reed, Phys. Rev. B **10**, 4765 (1974); M. Umehara, Phys. Rev. B **60**, 445 (1999).

[41] S. Broderick, B. Ruzicka, L. Degiorgi, H.R. Ott, J.L. Sarrao, and Z. Fisk, Phys. Rev. B **65**, 121102 (2002), and references therein.

[42] Such a wave function does not necessarily have to be a Bloch wave. In a purely 1D case, this would be a cosine wave, and it is also important that its wave vector will have to be related to the energy of the localized state by the usual tight-binding dispersion relation. We note that the choice of the basic set of electron energy eigenstates used in the Lifshits-Krein trace formalism [cf. Eqs. (29) and (31)] is, in principle, arbitrary.

[43] We consider the single-band case [cf. Eq. (1)], when the carriers originate solely from doping, and not from band overlap.

[44] Some possible examples of antiferromagnetic phases are discussed in Ref. 22.

[45] F. Stern, Phys. Rev. Lett. **18**, 546 (1967); F. Stern and W.E. Howard, Phys. Rev. **163**, 816 (1967).

[46] A.L. Fetter, Ann. Phys. (N.Y.) **81**, 367 (1973).

[47] This requirement is perhaps somewhat relaxed in the case of a thin film, due to the power-law (rather than exponential—see Appendix B) decay of the screened Coulomb potential.

[48] A.S. Alexandrov and A.M. Bratkovsky, J. Phys.: Condens. Matter **11**, L531 (1999), and references therein.

[49] J.-H. Park, C.T. Chen, S.-W. Cheong, W. Bao, G. Meigs, V. Chakarian, and Y.U. Idzerda, Phys. Rev. Lett. **76**, 4215 (1996); D. S. Dessau and Z.-X. Shen, in *Colossal Magnetoresistive Oxides*, edited by Y. Tokura (Gordon and Breach, New York, 2000), and references therein.

[50] Strictly speaking, there is also a surface charge (and hence Coulomb energy) associated with the interphase boundary itself, which in this respect is similar to the abrupt domain walls considered in Sec. III. Throughout Sec. IV we omit these electrostatic corrections to the energies of abrupt and Bloch domain

walls and interphase boundaries. They are expected to be much smaller than the electrostatic energies of the large charged islands considered here.

[51] The numerical smallness of W (which can be estimated as half the energy of an abrupt domain wall; see in the text below) and the fact that the actual values of $\bar{\epsilon}$ are large result in the value of Δ_0 [see Eq. (41)] being small and, more generally, in $|\Omega_{FM} - \Omega_{AFM}| \ll |\Omega_{FM,AFM}|$. It is therefore consistent to assume $\Omega_{FM} = \Omega_{AFM}$ when evaluating abrupt wall energies and W.

[52] We recall that the interphase boundaries are expected to be abrupt (Ref. 22).

[53] V.A. Kashin and E.L. Nagaev, Zh. Eksp. Teor. Fiz. **66**, 2105 (1974) [Sov. Phys. JETP **39**, 1036 (1974)]; E.L. Nagaev, Phys. Rev. B **62**, 5751 (2000).

[54] This method is exact for the stripe phase in 3D.

[55] See, e.g., E. Eisenberg, R. Berkovits, D.A. Huse, and B.L. Altshuler, Phys. Rev. B **65**, 134437 (2002), Fig. 1.

[56] This holds within the Wigner-cell approximation for the stripe phase. Within a more rigorous treatment, S_s will vanish at a certain point near δ_c.

[57] Thus, the interphase boundaries within the film *can* be oriented perpendicular to the film plane.

[58] J. Krupka, R.G. Geyer, M. Kuhn, and J.H. Hinken, IEEE Trans. Microwave Theory Tech. **42**, 1886 (1994); T. Konaka, M. Sato, H. Asano, and S. Kubo, J. Supercond. **4**, 283 (1991).

[59] Although under certain conditions stripe wall formation may be possible in the opposite case of a thick film or bulk crystal (see below and Appendix B), there is no reason to expect that these conditions are satisfied for the thicker samples studied in Ref. 6.

[60] E. Sawaguchi, A. Kikuchi, and Y. Kodera, J. Phys. Soc. Jpn. **17**, 1666 (1962); T. Sakudo and H. Unoki, Phys. Rev. Lett. **26**, 851 (1971).

[61] The change of domain wall structure in the film may be further assisted by the well-known structural phase transition in strontium titanate, which takes place at about the same temperature [see G. Shirane and Y. Yamada, Phys. Rev. **177**, 858 (1969), and references therein; V.K. Vlasko-Vlasov, Y.K. Lin, D.J. Miller, U. Welp, G.W. Crabtree, and V.I. Nikitenko, Phys. Rev. Lett. **84**, 2239 (2000)].

[62] For very large values of Hund's rule coupling, $J_H \to \infty$, abrupt walls can also be stabilized at low hole doping, $1 - x \ll 1$. Because of an effective antiferromagnetism associated with the finite value of J_H in real systems (and reflected, e.g., in the antiferromagnetic ordering commonly observed in manganates at $1 - x \ll 1$), it is unlikely that this situation can be realized experimentally.

[63] M. Yamanaka and N. Nagaosa, J. Phys. Soc. Jpn. **65**, 3088 (1996).

[64] N.D. Mathur, G. Burnell, S.P. Isaac, T.J. Jackson, B.-S. Teo, J.L. MacManus-Driscoll, L.F. Cohen, J.E. Evetts, and M.G. Blamire, Nature (London) **387**, 266 (1997).

[65] Y.-A. Soh, P.G. Evans, Z. Cai, B. Lai, C.-Y. Kim, G. Aeppli, N.D. Mathur, M.G. Blamire, and E.D. Isaacs, J. Appl. Phys. **91**, 7742 (2002), and references therein.

[66] V.K. Vlasko-Vlasov, U. Welp, D.J. Miller, Y.K. Lin, and G.W. Crabtree, J. Appl. Phys. **91**, 7721 (2002).

[67] A. Biswas, M. Rajeswari, R.C. Srivastava, T. Venkatesan, R.L. Greene, Q. Lu, A.L. de Lozanne, and A.J. Millis, Phys. Rev. B **63**, 184424 (2001); A.P. Nosov and P. Strobel, Fiz. Met. Metalloved. **93** (3), 50 (2002) [Phys. Met. Metallogr. **93**, 239 (2002)].

[68] M. Pratzer, H.J. Elmers, M. Bode, O. Pietzsch, A. Kubetzka, and R. Wiesendanger, Phys. Rev. Lett. **87**, 127201 (2001); J. Stöhr, A. Scholl, T.J. Regan, S. Anders, J. Lüning, M.R. Scheinfein, H.A. Padmore, and R.L. White, *ibid.* **83**, 1862 (1999).

[69] Equations (A12) and (A13) correct misprints in expressions for related quantities, $W_G = S_d^{(0)}/2$ and $W_A = S_v^{(0)}/2$, published earlier in Ref. 22.